The Calculation of Interface Motion of a Surfactant-Laden Bubble in Stokes Flow

by

Jeffrey R. P. Gilmore

B. Sc. Trinity Western University, 2001

A THESIS SUBMITTED IN PARTIAL FULFILLMENT
OF THE REQUIREMENTS FOR THE DEGREE OF
MASTER OF SCIENCE
IN THE DEPARTMENT
OF
MATHEMATICS

SIMON FRASER UNIVERSITY
October, 2003

APPROVAL

Name: Jeffrey R. P. Gilmore

Degree: Master of Science

Title of thesis: The Calculation of Interface Motion of a Surfactant-Laden Bubble in Stokes Flow

Examining Committee: Dr. Ralf Wittenberg
Chair

Dr. Mary Catherine Kropinski
Senior Supervisor

Dr. Steven Ruuth

Dr. David J. Muraki
Internal/External Examiner

Date Approved: _____

Abstract

Simulating time-evolving bubbles in a slow viscous flow presents a challenging free boundary value problem. The fluid motion is described with the Stokes equations and the interface of the bubble is advanced using the kinematic condition. Limiting our model to two-dimensional flow, complex variable theory of the biharmonic equation is exploited to formulate the problem in terms of analytic functions. By finding these harmonic functions subject to certain conditions on the boundary of the domain, analytical solutions can be found for a class of polynomial initial bubble shapes. For bubbles with a more general initial shape, numerical calculation is necessary.

Numerical and analytical solutions have been found for bubbles with a constant surface tension. The case where the surface tension varies according to the concentration of a surface active agent (surfactant) coating on the bubble adds additional analytical and numerical complications. While some significant work has been done on this problem, there is still a need to develop efficient, robust and highly accurate numerical methods in order to handle large-scale problems of this nature. The focus of this work is to survey physical models and analytical solutions for the variable surfactant case. To compute the analytical solutions, we must numerically solve the partial differential equation for surfactant transport on the interface. Spectral methods are used. These solutions will in the future be used as test cases for the development of a high-speed, general purpose solver which employs integral equations coupled with the fast multipole method for the variable surfactant case.

Acknowledgments

I would like to thank the professors in the Department of Mathematics at Simon Fraser University who helped me overcome many obstacles in graduate school and devoted themselves to my education. Amoung them I would especially like to thank my supervisor, Dr. M.C.A. Kropinski, for steering my thesis in a fruitful direction, encouraging me to explore different fields in applied mathematics, and providing funding for this research. I would also like to express my gratitude to Dr. D. J. Muraki and Dr. J. H. Verner for their inspiration and enthusiastic investment in the graduate students. My first graduate course with Dr. Muraki will remain a token memory of graduate school. And finally, many thanks to my family who have faithfully supported me through two university degrees.

Dedication

This thesis is dedicated to Mr. Miskall, my 6th grade math teacher who believed I would succeed in mathematics.

Contents

Abstract iii
Acknowledgments iv
Dedication v
Contents vi
List of Figures viii
1 Introduction 1
2 Mathematical Models 3
2.1 Slow Viscous Flow 3
2.2 Domain Geometry 5
2.3 Boundary Conditions: Clean-Flow 6
2.4 Boundary Conditions: Surfactant 8
2.4.1 Modified Boundary Conditions 9
2.4.2 Surfactant Transport 11
3 Biharmonic Theory and Analytical Solutions 14
3.1 The Biharmonic Equation and Complex Analysis 14
3.2 Goursat Function Formulation 19
3.3 Polynomial Analytical Solutions 24
3.3.1 Collapsing Bubbles in a Quiescent Flow 26
3.3.2 A Non-collapsing Bubble in Pure Straining Flow 29
4 Surfactant and Analytical Solutions 34
4.1 Modified Analytical Solutions 34
4.2 Surfactant Transport in Complex Variables 36
4.3 Computed Solutions 39
4.3.1 Collapsing Bubbles 41

4.3.2 Pure Straining Flow 49
5 Conclusion 52
Bibliography 54

List of Figures

2.1 A viscous fluid domain D with interface Γ 5

3.1 A collapsing 4-fold symmetric bubble with initial parameters $a(0) = 0.9$, $b_N(0) = 0.1$, initial area $A(0) = 0.78\pi$, and contraction rate $m = -2\pi$. It evolves until $t = 0.368$. 28
3.2 κ^* approaching infinity as t approaches $t = 0.39$ 28
3.3 Taylor's four-roller mill. 30
3.4 On the top, a circular bubble with initial parameters $a(0) = 1$, $b(0) = 0$, capillary number $C = 0.5$, and area $A = \pi$ placed in a pure straining flow approaches steady-state. On the bottom, $C = 0.7$; an unsteady solution. The bubble evolves until $t = 12$. 33

4.1 Simulation 1: Evolution of surfactant concentration on a collapsing four-fold symmetric bubble. The topmost profile is at $t = 0.28$. 42
4.2 Collapsing four-fold symmetric bubbles. On the left, a surfactant laden bubble with $\beta = 0.5$ (simulation 1). On the right, a clean bubble. The inner profiles are at $t = 0.28$. 43
4.3 Simulation 2: Evolution of surfactant concentration. The topmost profile is at $t = 0.28$. 44
4.4 Close up comparison from left to right: A clean bubble, simulation 1, and simulation 2. The innermost profiles are at $t = 0.28$. 45
4.5 Simulation 3: Evolution of surfactant concentration until $t = 0.339$. 47
4.6 Magnification of the fourth spike in figure (4.5) 47
4.7 Simulation 3: A bubble collapses until $t = 0.339$. 48
4.8 Close up comparison: a clean bubble, and simulation 3 (4.7) 48

4.9 Pure Strain: Evolution of surfactant concentration. Final profile at $t = 2$. . . 50
4.10 Pure Strain: Evolution of an initially circular bubble. Final profile at $t = 2$. . 50

Chapter 1

Introduction

Understanding the deformation of drops and bubbles in a slow viscous flow has practical application in the rheology of emulsions, and mixing in multiphase viscous systems. While in physical applications it would be preferable to have solutions for a three-dimensional drop or bubble, these are difficult to obtain both analytically and computationally. Significant work has been done, however, on the simplified model of two-dimensional drops and bubbles. Two-dimensional models are found to behave similarly to the corresponding three-dimensional bubbles observed in experiments [3]. Therefore, our study should prove useful in understanding bubbles in the real world.

In one analytical study, Tanveer and Vasconcelos [26] obtained a restricted class of analytical solutions to the two-dimensional problem. Since in two-dimensions the Stokes equations reduce to the biharmonic equation, these authors exploit an extensive complex theory of the biharmonic equation (cf. Mikhlin [19], Muskhelishvili [20], and Carrier, Krook, and Pearson [6]) to formulate the problem in terms of complex analytic functions. By finding these harmonic functions subject to certain conditions on the boundary, they present analytical solutions for a class of polynomial initial bubble shapes. The need to represent the bubble as a polynomial, however, limits the scope of these solutions. In particular, general bubble shapes and multiple bubble interactions cannot be developed by this approach.

In recent work, Kropinski [15, 16] overcomes both of these limitations by computing the evolution of drops and bubbles numerically. These computations feature an accurate and efficient integral equation method for the biharmonic equation developed by Greengard, Kropinski, and Mayo [12]. This method uses the above mentioned complex theory to formulate the Sherman-Lauricella integral equation. The discretization of the integral equation is

spectrally accurate and the matrix-vector products are computed using the fast multipole method [8]. Using N points to discretize the boundary, this method requires only $\mathcal{O}(N)$ operations compared to direct matrix inversion, which is $\mathcal{O}(N^3)$. Granted that the Stokes equations must be solved at each time-step, this reduction in computation is necessary for large scale simulations.

These computations are limited in that surface tension is constant. In the case where a bubble is coated with a surface active agent (surfactant), for example, surface tension varies. Analytical solutions have been investigated by Siegel [23, 24] and numerical solutions by Johnson and Borhan [14] and Pozrikidis [21]. There is still a need, however, to develop efficient, robust, and highly accurate numerical methods for the varying surface tension case, of the kind developed in [15].

The focus of this work is to survey mathematical models and analytical solutions for the variable surface tension, or surfactant, case. Incorporating surfactant involves an additional term in the stress balance on the interface [23], and solving a convective-diffusive partial differential equation for the evolution of surfactant concentration [28]. The nature of the domain lends this problem to fast Fourier transforms and spectral methods. These solutions are useful test cases for the future development of a high-speed, general purpose solver such as that in [15].

In chapter 2, we look at mathematical models of time-evolving bubbles in a slow viscous flow. First, the governing equations are derived from the more general Navier-Stokes equations. The domain geometry is described. Then the boundary conditions particular to constant and variable surface tension are defined and the transport equation for surfactant is derived. All relevant equations are presented in non-dimensional form.

In chapter 3, we examine analytical solutions to the constant surface tension problem. First, the biharmonic theory and complex analysis associated with the Goursat representation is developed. Then, a set of ordinary differential equations comprising a class of polynomial solutions are derived. Examples follow, including a collapsing bubble placed within a quiescent flow and a constant area bubble placed within a pure strain flow.

In chapter 4, the previous analytical solution theory is elaborated to account for the variable surface tension case. The surfactant transport equation is composed in complex variables consistent with previous analytical solutions. Some examples are then considered.

Finally, a summary of our results and potential problems for future research are presented in chapter 5.

Chapter 2

Mathematical Models

In this chapter, we present the equations and boundary conditions comprising the mathematical models considered in our study. Many of these equations come from well known scientific laws and it is assumed the reader has a familiarity with them. Wherever possible, elaboration on the physical concepts is provided. We follow the models presented by Tanveer and Vasconcelos [26] and Kropinski [15] for the constant surface tension (no surfactant) problem, and Siegel [23] for the variable surface tension problem. The surfactant-free case is also called *clean-flow*. We begin by describing the governing equations in slow viscous flow.

2.1 Slow Viscous Flow

Imagine being dropped into a pool of molasses and having to swim through it. The heavy, sticky fluid would impede one's movement because of the frictional forces in the fluid. It would be difficult to gain any momentum and glide as in aquatic swimming. Such dynamics are caused by the high viscosity of molasses. In another scenario, imagine looking through a microscope at a tiny organism propelling itself through a sample of pond scum. It might appear that the micro-organism must propel itself constantly to keep in motion. Water "seems" a great deal more viscous at a microscopic level. In this case, such dynamics are caused by the length scale. These two very different scenarios have a similar fluid dynamical behavior (known as slow viscous flow) because in both cases viscous forces dominate over inertial forces.

Newtonian fluids can be described generally using the Navier-Stokes equations. The

equations for slow viscous flow are a special case of the Navier-Stokes equations. A more thorough discussion of these equations can be found in [2]. If we assume the flow is incompressible we have

$$\mathbf{u}_t + (\mathbf{u} \cdot \nabla)\mathbf{u} = -\frac{1}{\rho}\nabla p + \nu \nabla^2 \mathbf{u}, \tag{2.1}$$

$$\nabla \cdot \mathbf{u} = 0, \tag{2.2}$$

where $\mathbf{u}$ is the velocity, p is the pressure, ρ is density, μ is viscosity, and $\nu = \mu/\rho$ is the kinematic viscosity. Suppose that U and L are characteristic values of velocity and length. Equation (2.1) can be non-dimensionalized with the following substitutions:

$$\begin{aligned} \mathbf{u} &= U\bar{\mathbf{u}}, \quad \mathbf{x} = L\bar{\mathbf{x}}, \\ p &= \frac{U\mu}{L}\bar{p}, \quad t = \frac{L}{U}\bar{t}. \end{aligned} \tag{2.3}$$

(2.1) now appears as

$$R[\bar{\mathbf{u}}_{\bar{t}} + (\bar{\mathbf{u}} \cdot \nabla)\bar{\mathbf{u}}] = -\nabla\bar{p} + \nabla^2\bar{\mathbf{u}},$$

where

$$R = \frac{UL}{\nu}$$

is the Reynolds number, and spatial derivatives are taken to be non-dimensional. R turns out to be the ratio of inertial forces to viscous forces. The value of this number characterizes the nature of the flow. When R is small ($R \ll 1$), the inertial terms become negligible and the viscous and pressure terms dominate the flow. By contrast, when R is large ($R \gg 1$) the viscous forces are dwarfed and inertial forces dominate, as in atmospheric and supersonic flows. Thus, small R is the appropriate case to consider. Low Reynolds number flow is also known as slow viscous flow and is given by the Stokes equations (with bars dropped):

$$\nabla p = \nabla^2 \mathbf{u} \tag{2.4}$$

$$\nabla \cdot \mathbf{u} = 0. \tag{2.5}$$

2.2 Domain Geometry

With the governing equations of slow viscous flow, we now consider the problem of a bubble placed in a two-dimensional flow of this type. Another example assists an intuition of the problem. Imagine blowing through a straw into a jar of molasses. An air bubble will expand and possibly separate from the straw. Motion in the fluid will interact with the fluid/bubble interface causing it to deform. If one took a horizontal cross section of the bubble, one could track the deformation of the bubble from an aerial point of view in two-dimensions.

From now on, general vector notation is taken to be two-dimensional. In two-dimensions, $\mathbf{u}(x, y) = (u, v, 0)$. We assume that the fluid inside the bubble has a negligible viscosity and is at a constant pressure, chosen to be zero without loss of generality (since it is the difference in pressure across the interface that matters). To be more general we could consider drops instead of bubbles, where the viscosity of the interior fluid is not negligible (as in [15]). In this case, we would be required to solve the Stokes equations on both sides of the interface. In the case of bubbles, however, the interior flow equations are trivially satisfied. The fluid domain is therefore exterior to the bubble.

Figure (2.1) below illustrates the fluid domain, and other geometrical details of the problem. The unit normal $\mathbf{n}$ points out of the fluid domain (into the bubble), and the unit tangent $\mathbf{s}$ points in the clockwise direction. θ is the angle between the horizontal axis and $\mathbf{s}$. The local curvature is given by $\kappa = \theta_s$, where s is the arclength increasing in a clockwise direction.

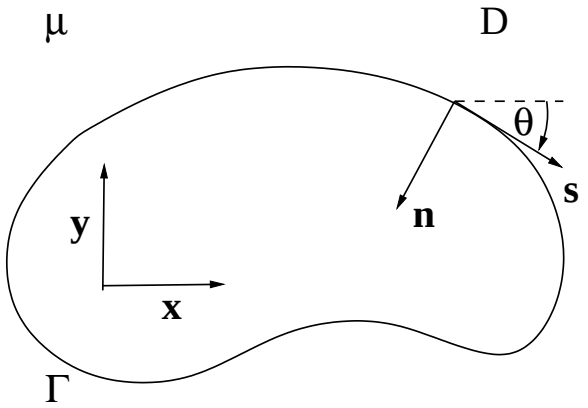

Figure 2.1: A viscous fluid domain D with interface Γ

2.3 Boundary Conditions: Clean-Flow

Boundary conditions (BCs) for this problem are given on the bubble interface and in the far-field, as $|\mathbf{x}|$ approaches infinity. We consider first the interface boundary conditions. The bubble surface evolves in time making this a free or moving boundary value problem. Following [23] and [15], the boundary conditions on the bubble interface include continuity of shear stress and a jump in normal stress proportional to curvature. These two stress boundary conditions can be written as

$$-p\mathbf{n} + 2\mu\mathbf{E}\cdot\mathbf{n} = -\sigma_0\kappa\mathbf{n} + \Delta\rho g\mathbf{n}_g\cdot\mathbf{x}\mathbf{n}, \tag{2.6}$$

where $\mathbf{E}$ is the rate of strain tensor whose j, k component is given by

$$e_{j,k} = \frac{1}{2}\left(\frac{\partial u_j}{\partial x_k} + \frac{\partial u_k}{\partial x_j}\right). \tag{2.7}$$

Each of the indices j and k take on the values 1 or 2 corresponding to the x or y-directions, σ_0 is the constant surface tension, κ is the curvature, $\mathbf{n}_g$ is the unit vector in the direction of gravity, $\Delta\rho$ is the difference in density between the bubble and the exterior fluid, and g is acceleration due to gravity. We assume a constant surface tension σ_0 for the clean-flow problem, but will require more complicated boundary conditions with the introduction of surfactant into the model in section (2.4).

In addition, we account for the effects of gravity on the stress interface condition as in [16]. Our analytical solutions neglect the effect of gravity ($g = 0$) but we include it in our mathematical model for completeness. We have not included body forces in our derivation of the equations of slow viscous flow, but gravity effects is absorbed into the pressure term by defining $p = \Pi - \rho g\mathbf{n}_g\cdot\mathbf{x}$, where Π is the dynamic pressure.

Turning our attention to the far-field condition, we assume that far from the bubble the velocity of the incident flow is linear, and the area of the bubble A is changing at a prescribed rate m, which may depend on time. The far-field condition appears as

$$\mathbf{u} \sim \mathbf{u}_\infty + \frac{m}{2\pi}\frac{\hat{\mathbf{x}}}{|\mathbf{x}|} + \mathcal{O}(1/|\mathbf{x}|^2) \quad \text{for} \quad |\mathbf{x}| \to \infty, \tag{2.8}$$

where $\hat{\mathbf{x}}$ is a unit vector in direction $\mathbf{x}$ when $|\mathbf{x}| \to \infty$ (usually unit vectors will be designated

with bold type), and

$$\mathbf{u}_\infty = \tfrac{1}{2}\begin{pmatrix} \alpha_0 & \beta_0 - \omega_0 \\ \beta_0 + \omega_0 & -\alpha_0 \end{pmatrix} \cdot \mathbf{x}. \tag{2.9}$$

Here ω_0 is the vorticity of the far-field flow, while α_0 and β_0 characterize its strain rate.

These conditions determine the solution to the boundary value problem associated with the Stokes equations (2.4, 2.5). We can in principle determine the velocity $\mathbf{u}$ in the exterior domain, particularly on the bubble interface. But this is a steady-state solution; how is the time-evolution of the bubble interface determined? After solving the Stokes equations, we employ the kinematic condition that a point $\mathbf{x}$ on the interface advances according to the normal velocity at that point, or

$$\frac{\mathrm{d}\mathbf{x}}{\mathrm{d}t} = (\mathbf{u}\cdot\mathbf{n})\mathbf{n}, \quad \mathbf{x} \in \Gamma. \tag{2.10}$$

In other words, we solve a sequence of steady-state boundary value problems to evolve the the bubble in time. This is known as a *quasistatic* problem.

In a previous section we obtained the non-dimensional Stokes equations; now we complete the problem description by presenting non-dimensional boundary conditions. We left some ambiguity in our choice of characteristic values (2.3) and we now choose the characteristic value U to be

$$U = \frac{\sigma_0}{\mu}. \tag{2.11}$$

This choice conveniently removes characteristic values from the stress interface condition. We now non-dimensionalize pressure and time by

$$\begin{aligned} p &= \frac{\sigma_0}{L}\bar{p} \\ t &= \frac{L\mu}{\sigma_0}\bar{t}. \end{aligned} \tag{2.12}$$

This permits us to eliminate σ_0 and μ from the boundary conditions. The stress interface

condition becomes

$$-\frac{\sigma_0}{L}\bar{p}\mathbf{n} + 2\frac{\sigma_0}{L}\overline{\mathbf{S}}\cdot\mathbf{n} = -\frac{\sigma_0}{L}\bar{\kappa}\mathbf{n} + \Delta\rho g L\mathbf{n}_g\cdot\bar{\mathbf{x}}\mathbf{n}.$$
$$-p\mathbf{n} + 2\mathbf{S}\cdot\mathbf{n} = -\kappa\mathbf{n} + \mathcal{B}\mathbf{n}_g\cdot\mathbf{x}\mathbf{n}, \tag{2.13}$$

where the bars have been dropped for convenience. Here, $\mathcal{B}$ is the Bond number,

$$\mathcal{B} = \frac{\Delta\rho g L^2}{\sigma_0},$$

The appearance of the far-field condition (2.8) remains unchanged, however we non-dimensionalize the rate of contraction by

$$m = \frac{\sigma_0 L}{\mu}\bar{m},$$

and drop the bar as before. If we wish to study the zero surface tension case [26], these choices in characteristic quantities for non-dimensionalization will not work, since there will be division by zero. It may be preferable to leave the problem in dimensional form.

2.4 Boundary Conditions: Surfactant

A degree of complexity can be added to our model of a time-evolving bubble in a slow viscous flow if we consider the presence of an agent on the interface of the bubble/fluid regions. *Surfactant* (i.e. a surface active agent) is simply a coating on the bubble that modifies surface tension (σ), but does not affect the flow of the exterior fluid directly. It will therefore modify the stress-interface boundary condition (2.13). The motion of the exterior fluid causes the convection of surfactant around the bubble, but surfactant will not be treated as part of the fluid domain influencing the exterior flow.

The addition of surfactant is helpful for studying interesting phenomena in fluid dynamics. In laboratory experiments, scientists observe how the physical addition of surfactant modifies the behaviour of a bubble in a viscous fluid. Because the interfacial tension is sensitive to the presence of even small amounts of surfactant, they play an important role in many free-boundary problems. For example, surfactant can increase the drag on translating drops [14], or damp wave motion [25]. In other cases, surfactant may promote the development of *cusps*, or point-like regions attaining an infinite curvature. Michael Siegel

[23] investigated the influence of surfactant on cusp formation and tip streaming:

> "Tip streaming is a mode of breakup in which a drop develops a deformed shape featuring cusp-like ends, from which small drops are emitted into the exterior fluid (see, e.g., [9, 11, 22] for experimental results). The shear or strain rate required for this type of breakup is typically much less than that required for the normal mode of breakup (fracture), in which a drop ruptures into two or three pieces of similar size, with a few tiny satellite drops in between. [9] Furthermore, the droplets produced by tip streaming can be much smaller than those produced by fracture. The experiments of [9] provide strong evidence that tip streaming occurs when interfacial tension gradients develop due to the presence of surfactant. Therefore, it is vital to take the influence of surfactant into account when examining the various modes of breakup in a drop exposed to shearing or straining flows."

Siegel goes on to capture this behavior mathematically and produces analytical bubble solutions with cusp-like features. Other interesting effects include the accumulation of surfactant in stagnant caps at the rear of translating or deforming bubbles. Johnson and Borhan [14] write

> "When surface convection is the predominant mechanism for surfactant transport on the interface, and the surfactant flux from the bulk [or exterior fluid domain] is extremely slow compared to the surface convective flux (i.e., in the limit of an insoluble surfactant monolayer), the interface is partitioned into a surfactant-free region near the leading end of the drop and a surfactant-saturated region near the trailing end which behaves like a stagnant cap."

Our model does not account for the flux of surfactant to and from the exterior fluid domain and so it may be possible to compute surfactant caps. This is investigated in section (4.3.2).

Below, we incorporate surfactant into our mathematical model by modifying the stress-interface condition, and then present the convection-diffusion equation governing surfactant movement around the bubble.

2.4.1 Modified Boundary Conditions

How is it that surfactant influences bubble or drop mechanics? In an investigation of the effects of surfactant on the mobility of rising/falling drops, Johnson and Borhan [14] offer a

helpful explanation:

> "Surfactants alter the mechanics of interfaces and, as such, their presence can have a profound effect on the macroscopic behavior of drops [10]. For instance, it is well known that the free rise/fall of drops can be significantly hindered by the presence of surfactants in the bulk phase... In this process, a nonuniform surfactant concentration profile is developed on the surface of the drop. If the only effect of surfactant is assumed to be a local reduction in the interfacial tension, the interface will be pulled from the low tension (high surfactant concentration) region at the rear pole to the high tension (low surfactant concentration) region. The resulting tangential (Marangoni) stress resists the surface flow, and eventually causes the interface to behave like a no-slip surface, thereby increasing the drag on the drop and reducing its mobility."

The above mentioned Marangoni forces are accounted for in [23] with an additional term in the stress-interface condition (2.6). σ represents the non-uniform surface tension and is non-dimensionalized by σ_0, chosen to be a characteristic value for surface tension (the same dimensional quantity chosen in the clean-flow problem). In non-dimensional form, the new stress-interface condition is

$$-p\mathbf{n} + 2\mathbf{S}\cdot\mathbf{n} = -\sigma\kappa\mathbf{n} + \nabla_s\sigma + \mathcal{B}\mathbf{n}_g\cdot\mathbf{n}. \tag{2.14}$$

Here, $\nabla_s = (\mathbf{I}-\mathbf{nn^t})\cdot\nabla$ is the surface gradient, which in two dimensions is a scalar derivative with respect to arclength. The non-uniformity of surface tension arises from its dependence on surfactant concentration Λ. This is given by an equation of state of the form

$$\sigma = \sigma(\Lambda).$$

Surfactant concentration is expressed in units of mass of surfactant per unit of interfacial length, and is non-dimensionalized with the uniform concentration of surfactant that exists in the absence of flow, Λ_0. Though more complicated equations of state might be proposed, we assume a linear relationship (in non-dimensional form) here:

$$\sigma = 1 - \beta\Lambda. \tag{2.15}$$

β is a parameter that controls the degree of sensitivity of surface tension to changes in the concentration of surfactant. This linear equation of state is simple, widely used, and useful, but it can easily be changed without disrupting the model presented.

2.4.2 Surfactant Transport

As the exterior fluid moves about the bubble, surfactant concentration will be spread across the bubble in a non-uniform layer. Other effects, like diffusion, and the evolution of the interface will change the distribution of surfactant as well. An equation for the evolution of surfactant must be coupled with the slow flow equations to complete our mathematical model. Stone [25] presents a simple derivation for the transport of surfactant along a deforming interface, which we use as a guide.

We consider a bubble interface Γ with a distribution of surfactant concentration Λ on it. Γ may be deforming. If we assume that surfactant is conserved, i.e. no diffusion, gain, or loss of surfactant into the surrounding fluid, a mass balance yields

$$\frac{\mathrm{d}}{\mathrm{d}t}\int_{\Gamma(t)} \Lambda d\Gamma = 0, \tag{2.16}$$

where d/dt denotes the material derivative. Proceeding formally, we may differentiate inside the integral:

$$\int_{\Gamma(t)} \left(\frac{\mathrm{d}\Lambda}{\mathrm{d}t} d\Gamma + \Lambda \frac{\mathrm{d}}{\mathrm{d}t} d\Gamma \right) = 0, \tag{2.17}$$

where the first term expresses the change in Λ from the perspective of a moving particle, and the second term accounts for stretching and distortion of the interface. By the definition of the material derivative, and the fact that Λ is only defined along the interface,

$$\frac{\mathrm{d}\Lambda}{\mathrm{d}t} = \frac{\partial \Lambda}{\partial t} + S \cdot \nabla_s \Lambda, \tag{2.18}$$

where $S = \mathbf{u} \cdot \mathbf{s}$.

Following the presentation in Stone [25] we deduce that the material derivative of a vector interface length $d\mathbf{\Gamma}$ is

$$\frac{\mathrm{d}}{\mathrm{d}t} d\mathbf{\Gamma} = d\mathbf{\Gamma} \nabla \cdot \mathbf{u} - (\nabla \mathbf{u}) \cdot d\mathbf{\Gamma}. \tag{2.19}$$

Substituting $d\mathbf{\Gamma} = \mathbf{n}d\Gamma$, and taking the inner product with $\mathbf{n}$, we have

$$\frac{\mathrm{d}}{\mathrm{d}t}d\Gamma = d\Gamma\nabla_s \cdot \mathbf{u}. \tag{2.20}$$

Returning to (2.17) we expand the material derivatives, and note that because $\Gamma(t)$ is arbitrary we isolate the integrand:

$$\int_{\Gamma(t)} \left(\frac{\partial \Lambda}{\partial t} + S \cdot \nabla_s \Lambda + \Lambda \nabla_s \cdot \mathbf{u} \right) d\Gamma = 0,$$

$$\frac{\partial \Lambda}{\partial t} + \nabla_s \cdot (\Lambda \mathbf{u}) = 0. \tag{2.21}$$

Next, we decompose $\mathbf{u}$ into its components tangential and normal to the surface: $\mathbf{u} = S\mathbf{s} + U\mathbf{n}$,

$$\frac{\partial \Lambda}{\partial t} + \nabla_s \cdot (\Lambda S) + \Lambda(\nabla_s \cdot \mathbf{n})(\mathbf{u} \cdot \mathbf{n}) = 0. \tag{2.22}$$

We note that $\nabla_s \cdot (\Lambda S) = \nabla_s \cdot (\Lambda \mathbf{u})$ and write

$$\frac{\partial \Lambda}{\partial t} + \nabla_s \cdot (\Lambda \mathbf{u}) + \Lambda(\nabla_s \cdot \mathbf{n})(\mathbf{u} \cdot \mathbf{n}) = 0. \tag{2.23}$$

Within the last term, $\nabla \cdot \mathbf{n}$ is equivalent to the mean curvature κ. When we add another term for diffusion across the interface, we have

$$\frac{\partial \Lambda}{\partial t} + \nabla_s \cdot (\Lambda \mathbf{u}) + \Lambda(\nabla_s \cdot \mathbf{n})(\mathbf{u} \cdot \mathbf{n}) = D_s \nabla_s^2 \Lambda, \tag{2.24}$$

where D_s is the diffusion constant.

The previous derivation provided by Stone [25] is simple and intuitive, but it leaves the nature of the unsteady time derivative ambiguous, as Wong, Rumschitzki, and Maldarelli have shown [28]. With the use of differential geometry, they show that it is necessary to include an additional term to account for the changing Lagrangian coordinate system, i.e. the bubble interface. The corrected equation is

$$\frac{\partial \Lambda}{\partial t} - \frac{\partial \mathbf{x}}{\partial t} \cdot \nabla_s \Lambda + \nabla_s \cdot (\Lambda \mathbf{u}) + \Lambda(\nabla_s \cdot \mathbf{n})(\mathbf{u} \cdot \mathbf{n}) = D_s \nabla_s^2 \Lambda. \tag{2.25}$$

Finally, we non-dimensionalize this equation to get

$$\frac{\Lambda_0\sigma_0}{L\mu}\frac{\partial\bar{\Lambda}}{\partial\bar{t}} - \frac{\sigma_0\Lambda_0}{L\mu}\frac{\partial\overline{\mathbf{x}}}{\partial\bar{t}}\cdot\nabla_s\bar{\Lambda} + \frac{\Lambda_0\sigma_0}{L\mu}\nabla_s\cdot(\bar{\Lambda}\overline{\mathbf{u}}) + \frac{\Lambda_0\sigma_0}{L\mu}\bar{\Lambda}(\nabla_s\cdot\mathbf{n})(\overline{\mathbf{u}}\cdot\mathbf{n}) = \frac{D_s\Lambda_0}{L^2}\nabla_s^2\bar{\Lambda}$$

$$\frac{\partial\Lambda}{\partial t} - \frac{\partial\mathbf{x}}{\partial t}\cdot\nabla_s\Lambda + \nabla_s\cdot(\Lambda\mathbf{u}) + \Lambda(\nabla_s\cdot\mathbf{n})(\mathbf{u}\cdot\mathbf{n}) = \frac{1}{Pe_s}\nabla_s^2\Lambda, \tag{2.26}$$

where Pe_s is the surface Peclet number

$$Pe_s = \frac{\sigma_0 L}{\mu D_s}. \tag{2.27}$$

The surface Peclet number can be thought of as the parameter that controls diffusion. In our numerical simulations, we choose large Pe_s so that the effects of diffusion are minimal.

Chapter 3

Biharmonic Theory and Analytical Solutions

A general class of analytical solutions for a time-evolving bubble in a two-dimensional slow viscous flow is presented by Tanveer and Vasconcelos [26]. These "clean" solutions do not take into account the variation in surface tension caused by surfactant. Following [26], we consider the more basic model presented in section (2.3). We develop the solution method they outline and seek to present the theory behind it including complex variables and the biharmonic equation, the Goursat representation, complex Poisson's formula, and complete elliptical integrals of the first kind. Several solution examples will be given, including a collapsing four-fold bubble that develops cusps, and a bubble placed within a pure straining flow. Similar computations have been performed in [15, 26].

3.1 The Biharmonic Equation and Complex Analysis

The clean flow problem, specified by the Stokes equations (2.4, 2.5) and appropriate boundary conditions, can be reformulated in terms of a scalar stream function W (This calculation has been previously completed by Acheson [2] and Langlois [18]). The benefit of this formulation is that the information of the vectorized Stokes equations can be concisely represented with one scalar equation. This comes as a consequence of the incompressibility condition

$\nabla \cdot \mathbf{u}$ (2.5), and restriction to two dimensions. Since $\nabla \cdot \mathbf{u} = 0$, then $\mathbf{u}$ is solenoidal [17] and

$$\exists\ \mathbf{W} \ni \mathbf{u} = \nabla \times \mathbf{W}. \tag{3.1}$$

Because $\mathbf{u}$ is two-dimensional,

$$\begin{aligned} \mathbf{W} &= W\mathbf{k} \\ \mathbf{u} &= \nabla \times W\mathbf{k} \\ u &= W_y, \quad v = -W_x, \end{aligned} \tag{3.2}$$

where $\mathbf{k}$ is the unit normal pointing out of the plane. By substituting W into the Stokes equation, we see that for creeping flows the stream function satisfies the biharmonic equation:

$$\begin{aligned} \nabla^2(\nabla \times W\mathbf{k}) &= \nabla p \\ \nabla \times \nabla^2(\nabla \times W\mathbf{k}) &= \nabla \times \nabla p \\ \nabla^2(\nabla \times \nabla \times W\mathbf{k}) &= 0 \\ \nabla^4 W &= 0. \end{aligned} \tag{3.3}$$

In the case at hand the curl operator may be taken into the quantity on the left hand side, but this is not a general identity. There is a complex variable theory for the biharmonic equation that can be exploited to derive analytical solutions [23, 26] or numerical methods [15]. We outline this theory here.

It follows from (3.3) that $\nabla^2 W$ is harmonic; that is, it satisfies Laplace's equation:

$$\nabla^2(\nabla^2 W) = 0. \tag{3.4}$$

We introduce vorticity, defined

$$\begin{aligned} \omega &= \nabla \times \mathbf{u} \\ &= \nabla \times \nabla \times W\mathbf{k} \\ &= v_x - u_y \qquad (3.5) \\ &= \omega\mathbf{k}. \qquad (3.6) \end{aligned}$$

We see that this function is the component of vorticity pointing out of the plane (the only component of vorticity in two-dimensional flow). When we apply the Laplacian operator (∇^2) to the definition of W (3.2) we find

$$\begin{aligned}\nabla^2 W = W_{xx} + W_{yy} &= -v_x + u_y \\ &= -\omega.\end{aligned}$$

Hence, it follows from 3.4 that ω is a harmonic function:

$$\nabla^2 \omega = 0 \tag{3.7}$$

Now, consider pressure. Applying the divergence operator to the Stokes equation (2.4) we find

$$\begin{aligned}\nabla \cdot (\nabla p) &= \nabla \cdot (\nabla^2 \mathbf{u}) \\ \nabla^2 p &= \nabla^2 (\nabla \cdot \mathbf{u}) \\ \nabla^2 p &= 0,\end{aligned} \tag{3.8}$$

where the last step is accomplished with the incompressibility condition (2.5). Hence, p is a harmonic function as well. With further calculations, we can show that ω and p are the components of a complex analytic function.

From the definition of ω (3.6), observe

$$\begin{aligned}\omega &= v_x - u_y \\ \omega_x &= v_{xx} - u_{xy}.\end{aligned}$$

By the incompressibility condition (2.5),

$$-u_{xy} = v_{yy}$$

we find that

$$\omega_x = \nabla^2 v. \tag{3.9}$$

Following a similar calculation, we find

$$\omega_y = -\nabla^2 u. \tag{3.10}$$

Comparing (3.9) and (3.10) with Stokes' equation (2.4), we see that ω and p satisfy the Cauchy-Riemann equations:

$$\omega_x = p_y, \quad \omega_y = -p_x. \tag{3.11}$$

We observe that ω and p are *conjugate harmonic functions*; that is to say they satisfy (3.11) and as a result both satisfy Laplace's equation. This is the crucial step since the real and imaginary parts of a complex analytic function must be conjugate harmonic functions [6]. Thus, we can define an analytic function of z whose real and imaginary parts are ω and p. We define the function $\phi(z)$ to satisfy

$$-4\phi'(z) = \omega + ip, , \tag{3.12}$$

whereas its integral is also analytic,

$$-4\phi(z) = 4g(x,y) + 4i\tilde{g}(x,y). \tag{3.13}$$

Here, a prime indicates a derivative, and g and $\tilde{g}$ are the real and imaginary parts of $\phi(z)$. Implicit in this definition is the representation of the $x-y$ plane as the complex z-plane, with

$$\begin{aligned} z &= x + iy, \text{ and} \\ \mathbf{u} &= u + iv. \end{aligned} \tag{3.14}$$

Let us additionally define

$$G(x,y) = xg(x,y) + y\tilde{g}(x,y) + W. \tag{3.15}$$

Applying the Laplacian operator,

$$\begin{aligned}\nabla^2 G &= x\nabla^2 g + y\nabla^2 \tilde{g} + 2\left(g_x + \tilde{g}_y\right) + \nabla^2 W \\ &= 4g_x + \nabla^2 W = -4Re(\phi'(z)) + \nabla^2 W \\ &= \omega + \nabla^2 W = 0,\end{aligned}$$

and hence G is harmonic. We set G as the real part of complex analytic function χ,

$$\mathrm{Re}(\chi(z)) = G. \tag{3.16}$$

The imaginary part could be determined by the Cauchy-Riemann equations but is not of immediate consequence here. Rearranging (3.15), we have

$$\begin{aligned}W(x,y) &= \mathrm{Re}(\chi(z)) - [xg(x,y) + y\tilde{g}(x,y)] \\ &= \mathrm{Re}(\bar{z}\phi(z) + \chi(z)),\end{aligned} \tag{3.17}$$

where we have made use of the identity $xg + y\tilde{g} = -Re[\bar{z}\phi(z)]$, and a bar ($\bar{z}$) indicates a complex conjugate. We have now expressed the stream function W in terms of the analytic functions ϕ and χ. (3.17) is known as *Goursat's formula*.

We can find expression for all relevant physical quantities in terms of Goursat functions. Recall from the definition of ϕ (3.12),

$$p = -4\mathrm{Im}(\phi'(z)). \tag{3.18}$$

In a similar way we find velocity,

$$\begin{aligned}i(u+iv) &= i(W_y - iWx) \\ &= W_x + iW_y \\ &= \frac{\partial \mathrm{Re}(\bar{z}\phi(z) + \chi(z))}{\partial x} + i\frac{\partial \mathrm{Re}(\bar{z}\phi(z) + \chi(z))}{\partial y} \\ &= \mathrm{Re}(\phi(z) + \bar{z}\phi'(z) + \chi'(z)) + i\mathrm{Im}(\phi(z) - \bar{z}\phi'(z) - \chi'(z)) \\ &= \phi(z) + z\overline{\phi'(z)} + \overline{\chi'(z)}, \\ &= \phi(z) + z\overline{\phi'(z)} + \overline{\psi(z)},\end{aligned} \tag{3.19}$$

where we have defined $\psi(z) = \chi'(z)$. From (2.6) we find stress,

$$\begin{aligned} e_{11} &= u_x \\ &= -\mathrm{Im}(\bar{z}\phi''(z) + \psi'(z)) \\ e_{12} &= \tfrac{1}{2}(u_y + v_x) \\ &= -\mathrm{Re}(\bar{z}\phi''(z) + \psi'(z)) \\ e_{11} + ie_{12} &= i(z\overline{\phi''(z)} + \overline{\psi'(z)}). \end{aligned} \tag{3.20}$$

The analytic functions ϕ and ψ are known as *Goursat functions* [6, 18]. They are analytic, and hence harmonic functions in x and y. We solve for them in the fluid domain by solving Laplace's equation.

3.2 Goursat Function Formulation

With the preceding biharmonic and complex theory in place, we are equipped to investigate analytical solutions to the problem posed in (2.3). For these solutions our physical model is simplified by neglecting the influence of gravity and surfactant. We follow the solutions presented in [26].

The task of solving the governing equations has been reduced to finding the Goursat functions, $\phi(z)$ and $\psi(z)$. They must be chosen so that the boundary conditions are satisfied. For this, our original boundary conditions must be recomposed in order to produce conditions on the Goursat functions. Consider first the integral of (3.18) as z approaches infinity,

$$\phi(z) \sim -\frac{i}{4}[p_\infty(t) - i\omega_0]z - \frac{i}{4}B(t) + \mathcal{O}(1/z) \quad as \quad |z| \to \infty, \tag{3.21}$$

where p_∞ and $B(t)$ are to be determined. By rewriting the far-field condition (2.8) in terms of Goursat functions, and using (3.21) and (3.19) we find,

$$\psi(z) \sim -\frac{i}{2}(\alpha_0 - i\beta_0)z - i\bar{B}(t) - \frac{im}{2\pi z} + \mathcal{O}(1/z^2) \quad as \quad |z| \to \infty. \tag{3.22}$$

In this problem, it is convenient to define the unit normal vector on the surface of the

bubble,

$$\mathbf{n} = n_1 + in_2 = -i(x_s + iy_s) = -iz_s = -ie^{i\theta}, \tag{3.23}$$

where the arclength s increases in the clockwise direction and θ is the angle between the positive real axis and the tangent. We note that this is consistent with our geometric definition in section (2.2). Implicitly, we have also defined the unit tangent vector as z_s. Then, the two stress conditions (2.13) can be written as one equation:

$$-p\mathbf{n} + 2(e_{11} + ie_{12})\bar{\mathbf{n}} = -\kappa\mathbf{n}. \tag{3.24}$$

By inserting (3.18), (3.20), and (3.23) we rewrite the stress condition in terms of Goursat functions.

$$\begin{aligned} -p\mathbf{n} + 2(e_{11} + ie_{12})\bar{\mathbf{n}} &= 4\mathrm{Im}(\phi')(-iz_s) - 2i(z\overline{\phi''} + \overline{\psi'})(i\overline{z_s}) \\ &= 4\frac{(\phi' - \overline{\phi'})}{2i}(-iz_s) - 2i(z\overline{\phi''} + \overline{\psi'})(i\overline{z_s}) \\ &= -2(\phi' - \overline{\phi'})z_s + 2(z\overline{\phi''} + \overline{\psi'})\overline{z_s} \\ &= -2(\phi - z\overline{\phi'} - \overline{\psi})_s. \end{aligned} \tag{3.25}$$

This last step was accomplished with a careful use of the chain rule. Observe that

$$\begin{aligned} \frac{\partial\phi}{\partial s} &= \frac{\partial\phi}{\partial z}\frac{\partial z}{\partial s} = \phi'(z)z_s, \quad \text{but} \\ \frac{\partial\bar{\phi}}{\partial s} &= \frac{\partial\bar{\phi}}{\partial\bar{z}}\frac{\partial\bar{z}}{\partial s} = \overline{\phi'}(z)\bar{z}_s. \end{aligned}$$

When curvature is defined $\kappa = \theta_s$, we can write the right hand side of (3.24) as

$$\kappa\mathbf{n} = -\kappa ie^{i\theta} = -\theta_s(z_s)_\theta = -z_{ss}. \tag{3.26}$$

Integrating (3.25) with respect to s, we have

$$\phi - z\overline{\phi'} - \overline{\psi} = -\frac{z_s}{2}. \tag{3.27}$$

In terms of velocity, this reads

$$u + iv = -i\frac{z_s}{2} - 2i\phi. \tag{3.28}$$

We apply this stress condition on the bubble interface, which is irregularly shaped. It is a very difficult domain for either solving for the Goursat functions or applying an interface condition. By introducing a *conformal mapping* (angle magnitude and orientation remain the same [6]), however, we can map the shape of the bubble onto the unit circle. We define this as the ζ-plane and relate it to the z-plane (fluid domain) by the conformal mapping

$$z(\zeta, t) = \frac{a(t)}{\zeta} + h(\zeta, t). \tag{3.29}$$

$h(\zeta, t)$ is assumed analytic and $z_\zeta \neq 0$ in $|\zeta| \leq 1$ for at least some period of time. It maps the interior of the unit circle in the ζ-domain to the exterior of the bubble in the fluid domain. The $\zeta = 0$ point corresponds to $z = \infty$ in the fluid domain.

The advantage of using the Goursat formulation becomes clear here. Whereas the biharmonic equation is not preserved under conformal mappings, Laplace's equation is [18, 6]. It is by virtue of the fact that the problem is posed in terms of Goursat functions that we are able to map the solution from the unit circle to the fluid domain. Once a solution is obtained on the unit circle (independent of time), the evolving bubble is characterized by $a(t)$ and $h(\zeta, t)$.

Continuing with the kinematic condition (2.10), we write it as one complex equation

$$\begin{aligned}
\text{using} \quad \mathbf{u}\cdot\mathbf{n} &= un_1 + vn_2 = \mathrm{Re}((u+iv)\bar{\mathbf{n}}) \\
z_t - (\mathbf{u}\cdot\mathbf{n})\mathbf{n} &= 0 \\
\frac{z_t}{iz_s} - \mathrm{Im}\left(\frac{u+iv}{z_s}\right) &= 0 \\
\mathrm{Im}\left(\frac{z_t - (u+iv)}{z_s}\right) &= 0,
\end{aligned} \tag{3.30}$$

which holds on the unit circle ($|\zeta| = 1$). Another useful identity,

$$z_s = i\zeta z_\zeta/|z_\zeta| \quad \text{on} \quad |\zeta| = 1, \tag{3.31}$$

can be verified with $\bar{z}_s = 1/z_s$. Combining the stress condition (3.28) and (3.31) with the

kinematic condition (3.30), the following holds on $|\zeta| = 1$

$$\mathrm{Re}\left[\frac{z_t + 2i\Phi(\zeta,t)}{\zeta z_\zeta}\right] = \frac{1}{2|z_\zeta|} \equiv r(\zeta,t), \tag{3.32}$$

where

$$\Phi(\zeta,t) = \phi(z(\zeta,t),t),$$

and the right hand side of (3.32) is defined $r(\zeta,t)$ for convenience.

The analyticity of (3.32) depends on the analyticity of $\Phi(\zeta,t)$. As defined, Φ is analytic in $|\zeta| \leq 1$, except at the origin (corresponding to the far-field boundary condition). From (3.21) and (3.29), we see that it is a simple pole:

$$i\Phi(\zeta,t) \sim \frac{a(p_\infty - i\omega_0)}{4\zeta} + B(t) + \mathcal{O}(\zeta) \quad as \quad |\zeta| \leftarrow 0.$$

Fortunately the simple poles in the numerator and denominator cancel out, so that the quantity in the square brackets (3.32) has a removable singularity. Clearly, $r(\zeta,t)$ must also be analytic here. It follows that $r(\zeta,t)$ is a harmonic function. Since $r(\zeta,t)$ is specified on the boundary, we can solve for $r(\zeta,t)$ in $|\zeta| < 1$ as the solution to a well-posed Dirichlet problem:

$$\begin{aligned} \nabla^2 r &= 0 \qquad \text{in} \quad |\zeta| < 1 \\ r &= \frac{1}{2|z_\zeta|} \quad \text{on} \quad |\zeta| = 1. \end{aligned}$$

Poisson's formula provides the solution when $r(\zeta,t)$ is real, but it can be extended to complex analytic functions as well. For our problem, the given boundary data is real but there is implicitly an imaginary part of the boundary data determined by the Cauchy-Riemann equations. Suppose r is the real part of a complex function $R(\zeta,t) = r + i\tilde{r}$. The imaginary part, $\tilde{r}$, is then determined by the Cauchy-Riemann equations.

Since the imaginary part of R is thus constrained, we must specify only the real data on the boundary to obtain the analytic function R (providing both would likely contradict the Cauchy-Riemann equations). On the other hand, with the given data we could obtain a strictly real solution, but we want a complex solution in order to specify the complex analytic function Φ. Carrier [6] provides the complex analogue of Poisson's formula. For

$|\zeta| < 1$,

$$\begin{aligned} R(\zeta,t) &= iC + \oint_{|\zeta'|=1} r(\zeta',t)\left[\frac{\zeta'+\zeta}{\zeta'-\zeta}\right]\frac{d\zeta'}{\zeta'} \\ &= iC + \frac{1}{4\pi i}\oint_{|\zeta'|=1}\frac{1}{|z_\zeta(\zeta',t)|}\left[\frac{\zeta'+\zeta}{\zeta'-\zeta}\right]\frac{d\zeta'}{\zeta'} \\ &= iC + I(\zeta,t), \end{aligned} \tag{3.33}$$

where $C = \tilde{r}(\zeta = 0)$ and may be determined later. By analytic continuation of (3.32), we obtain an expression for $\Phi(\zeta,t)$ in $|\zeta| < 1$:

$$z_t + 2i\Phi(\zeta,t) = \zeta[I(\zeta,t) + iC]z_\zeta. \tag{3.34}$$

It may seem strange to construct $\Phi(\zeta,t)$ in this way, but it is sufficient as long as it satisfies the boundary conditions. By taking the limit as $\zeta \to 0$ in (3.34) and matching singular terms we find,

$$\begin{aligned} C &= \tfrac{1}{2}\omega_0, \\ p_\infty &= -2[I(0,t) + \frac{\dot{a}}{a}], \end{aligned}$$

where the dot denotes time derivative. We also seek an expression for ψ, our other Goursat function, in $|\zeta| < 1$. For convenience, define

$$\Psi(\zeta,t) = \psi(z(\zeta,t),t).$$

Examining (3.22) and (3.29) we note that $\Psi(\zeta,t)$ is analytic everywhere in $|\zeta| \leq 1$, except for a simple pole at $\zeta = 0$. Using (3.31) in the stress boundary condition (3.27) and taking the complex conjugate, we obtain

$$\Psi(\zeta,t) = -\bar{\Phi} - \bar{z}\frac{\Phi_\zeta}{z_\zeta} + \frac{1}{2}\frac{\bar{z}_\zeta^{1/2}}{\zeta z_\zeta} \tag{3.35}$$

where we use the fact that $\bar{\zeta} = 1/\zeta$ on $|\zeta| = 1$. As with (3.34), this holds on the boundary $|\zeta| = 1$ and becomes valid in $|\zeta| \leq 1$ by analytic continuation. We eliminate $\Phi(\zeta,t)$ from

this equation using (3.34), and simplify to obtain

$$2\Psi(\zeta,t) = \bar{z}\left\{\frac{z_{\zeta t}}{z_\zeta} - \zeta I_\zeta - \left[1 + \frac{\zeta z_{\zeta\zeta}}{z_\zeta}\right][I(\zeta,t) + iC]\right\} + \zeta^{-1}[I(\zeta,t) + iC]\bar{z}_\zeta + \bar{z}_t, \quad (3.36)$$

where we have made use of the fact that on $|\zeta| = 1$,

$$\begin{aligned} \mathrm{Re}I(\zeta,t) &= \frac{1}{2|z_\zeta|} \\ I + \bar{I} &= \frac{1}{z_\zeta^{1/2}\bar{z}_\zeta^{1/2}}. \end{aligned} \quad (3.37)$$

Much of the information in the original boundary value problem is concentrated in (3.36). In the next section, it is coupled the assumption that the bubble has a polynomial representation to generate a set of ordinary differential equations describing the motion of the bubble.

3.3 Polynomial Analytical Solutions

The constraint that (3.36) is analytic is imposed to derive evolution equations for the parameters characterizing the conformal mapping (3.29). In other words, the mapping function $z(\zeta,t)$ is determined by (3.36). To obtain a general class of solutions, we assume that the function $h(\zeta,t)$ (3.29) is a polynomial of degree N:

$$z(\zeta,t) = \frac{a(t)}{\zeta} + \sum_{j=1}^{N} b_j(t)\zeta^j. \quad (3.38)$$

The problem is now to find a set of evolution equations for the coefficients a and b_j. This is made possible with a procedure of matching singular terms in (3.36). First multiply (3.36) by z_ζ to obtain

$$2z_\zeta\Psi = z_\zeta\left\{\zeta^{-1}[I(\zeta,t) + iC]\bar{z}_\zeta + \bar{z}_t\right\} + \bar{z}\left\{z_{\zeta t} - \zeta I_\zeta z_\zeta - [z_\zeta + \zeta z_{\zeta\zeta}][I(\zeta,t) + iC]\right\}. \quad (3.39)$$

Using the far-field condition on G (3.22) and (3.29) we see that as $\zeta \to 0$ the singular

behavior of the left-hand side of (3.39) is

$$2z_\zeta \Psi \sim -\frac{a^2(\alpha_0 - i\beta_0)}{\zeta^3} - \frac{2a\bar{B}(t)}{\zeta^2} - \frac{m}{\pi\zeta} + \mathcal{O}(\zeta) \quad as \quad |\zeta| \to 0. \tag{3.40}$$

To find the singular terms on the right-hand side of (3.39), consider the Taylor series expansion of $I(\zeta, t)$:

$$I(\zeta, t) = I_0 + \sum_{j=1}^{\infty} \hat{I}_j(t)\zeta^j, \tag{3.41}$$

where the coefficients I_0 and $\hat{I}_j$, using (3.33), are

$$I_0 = \frac{1}{4\pi}\int_0^{2\pi} \frac{d\nu}{|z_\zeta(e^{i\nu}, t)|}, \tag{3.42}$$

$$\hat{I}_k = \frac{1}{2\pi}\int_0^{2\pi} \frac{e^{-ik\nu}}{|z_\zeta(e^{i\nu}, t)|} d\nu, \quad k \geq 1. \tag{3.43}$$

We define $\hat{I}_0 = I_0 + iC$ for simplicity, and $\zeta = e^{i\nu}$ on the unit circle in the ζ-plane so that it is parameterized in ν. It is now possible to expand the right-hand side of (3.39) as a polynomial in ζ and match with the singular terms on the left-hand side (3.40). This is a tedious procedure, the details of which can be consulted in [26]. The resulting system is conveniently written by defining the quantities c_k, (as in [23])

$$\begin{aligned}
c_{N+1} &= a\bar{b}_N, \\
c_N &= a\bar{b}_{N-1}, \\
c_k &= a\bar{b}_{k-1} - \sum_{j=1}^{N-k} j b_j \bar{b}_{k+j}, \quad 2 \leq k \leq N-1, \\
c_1 &= a^2 - \sum_{j=1}^{N} j|b_j|^2.
\end{aligned}$$

The ODEs then take the form

$$\dot{c}_1 = \frac{m}{\pi}, \tag{3.44}$$

$$\dot{c}_k = -k \sum_{j=0}^{N+1-k} \hat{I}_j c_{k+j+1} + a^2(\alpha_0 - i\beta_0)\delta_{k+1,3}, \quad 2 \leq k \leq N+1. \tag{3.45}$$

We note that the area enclosed by the bubble (the image of the unit circle) is given by $A = \pi c_1$. This set of ODEs forms a general class of analytical solutions to the clean-flow problem posed in (2). We must specify far-field flow (parameters $\alpha_0,\ \beta_0$) and the initial bubble shape ($a,\ b_j$) to find a particular solution. These ODEs can be solved approximately by standard numerical methods. We investigate a solution below.

3.3.1 Collapsing Bubbles in a Quiescent Flow

One of the solutions obtained by the Tanveer and Vasconcelos [26] is that of a contracting/expanding bubble in a *quiescent*, or undisturbed, flow. Physically, one could think of this as blowing/sucking air into/from the bubble. This corresponds to setting the coefficients of the external flow to zero, $\alpha_0 = \beta_0 = \omega_0 = 0$ (see (2.9)). The far-field behavior is then entirely governed by the contraction rate m, which we take to be a constant for simplicity. The coefficients b_j are taken to be real and a is real and negative. In addition, we choose $b_j = 0$ for $j < N$ so that

$$z(\zeta, t) = a(t)/\zeta + b_N(t)\zeta^N. \tag{3.46}$$

With this construction, $N = 1$ corresponds to an ellipse and $N > 1$ corresponds to $N+1$ fold symmetry. In this case, the set of ODEs (3.44, 3.45) reduces to one evolution equation given by

$$\frac{\mathrm{d}(ab_N)}{\mathrm{d}t} = -(N+1)I_0(a, b_N), \tag{3.47}$$

while the area condition, given by (3.44) after integration, is

$$A(t) = \pi[a^2 - Nb_N^2] = [A(0) + mt], \tag{3.48}$$

where the constant of integration, $A(0)$, is the initial bubble area.

As in [15], I_0 can be expressed as

$$\begin{aligned} I_0(a, b_N) &= \frac{1}{2\pi} \int_0^{\pi} \frac{d\nu}{\{a^2 + N^2 b_N^2 - 2Nab_N \cos(\nu)\}^{1/2}} \\ &= \frac{1}{\pi|a|} \frac{\rho}{\rho + 1} K \left[\frac{4\rho}{(1+\rho)^2} \right], \end{aligned} \tag{3.49}$$

where $\rho = a/Nb_N$, and K is the complete elliptic integral of the first kind defined (see Abramowitz and Stegun [1]) by

$$\begin{aligned} K(m) &= \int_0^1 [(1 - \bar{t}^2)(1 - m\bar{t}^2)]^{-1/2} d\bar{t} \\ &= \int_0^{\pi/2} (1 - m \ \sin^2 \bar{\theta})^{-1/2} d\bar{\theta}. \end{aligned}$$

It is helpful to express the evolution equation (3.47) as an ODE in one variable; we recompose it in ρ. Then we must express the other quantities in terms of ρ. Dividing (3.48) by a^2 we find

$$a^2 = N^2 \rho^2 b_N^2 = \frac{N\rho^2 A(t)}{\pi(N\rho^2 - 1)}, \tag{3.50}$$

$$(b_N^2)_t = \left(\frac{A(t)}{N\pi(N\rho^2 - 1)} \right)_t. \tag{3.51}$$

Then the evolution equation appears,

$$\begin{aligned} \frac{\mathrm{d}(\rho N b_N^2)}{\mathrm{d}t} &= \dot{\rho} N b_N^2 + N\rho (b_N^2)_t \\ &= -(N+1) I_0(a, b_N). \\ \dot{\rho} &= \rho \frac{N\rho^2 - 1}{N\rho^2 + 1} \left[(N+1) I_0 + \frac{m}{A} \right], \end{aligned} \tag{3.52}$$

after some simplification and collection of terms. The ODE for ρ specifies the evolution of a symmetric collapsing bubble in slow viscous flow.

One exact solution appears in figure (3.1). We integrate (3.52) with built-in MATLAB solver `ODE45` setting tolerance levels (RelTol) to 10^{-10}. Note the formation of cusps as the bubble collapses.

In theory, granted that the bubble has a non-zero surface tension (σ), the solution exists

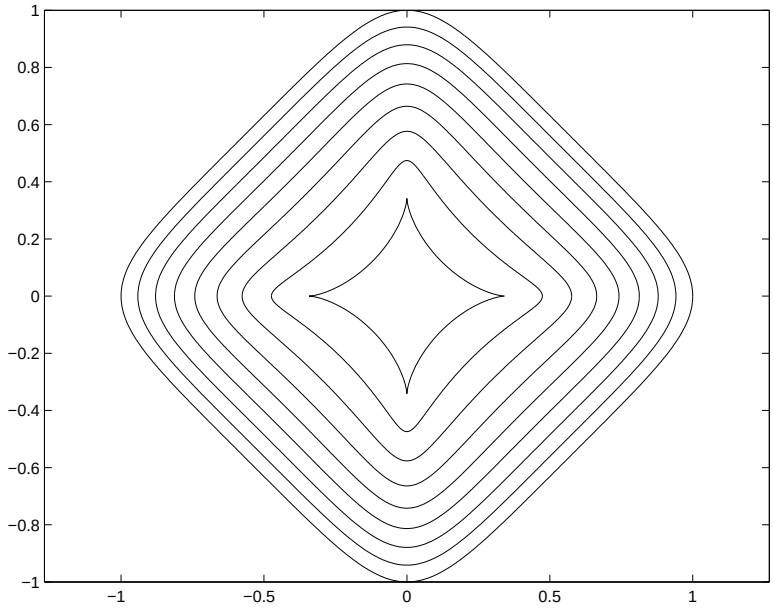

Figure 3.1: A collapsing 4-fold symmetric bubble with initial parameters $a(0) = 0.9$, $b_N(0) = 0.1$, initial area $A(0) = 0.78\pi$, and contraction rate $m = -2\pi$. It evolves until $t = 0.368$.

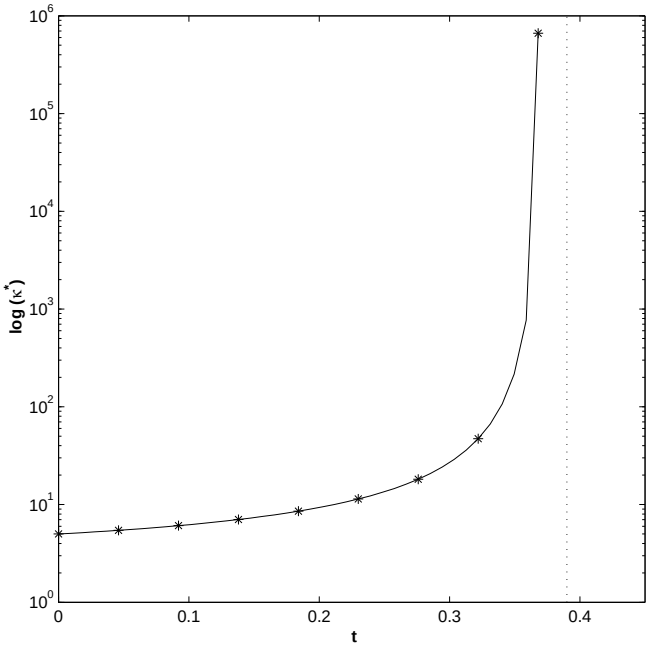

Figure 3.2: κ^* approaching infinity as t approaches $t = 0.39$

until all the air is removed from the bubble [26], at $t = 0.39$. It is at this time that curvature is infinite and a true cusp forms. According to Kropinski [15], we can compute the maximum curvature on the interface from

$$\kappa^*(t) = \frac{a(t) + b_N(t)N^2}{(a(t) - b_N(t)N)^2}. \tag{3.53}$$

Nevertheless, it is difficult to compute until all the air is removed since the magnitude of curvature becomes unmanageable for integration. The maximum curvatures for the computations in figure 3.1 are shown in figure 3.2.

This difficulty seems to be related to the computation of the complete elliptic integral of the second kind (3.49). As maximum curvature increases, ρ approaches the value 1^+, and the argument of K approaches the value 1^-, where K blows up. If we attempt to compute beyond this blow-up time, we find non-physical solutions where the interface crosses itself at the near-cusps.

In what sense are these solutions exact? We have avoided calling them "exact solutions," preferring "analytical solutions," because they have been computed numerically. Nevertheless, they are a vast improvement upon a fully numerical calculation involving spatial as well as time integration. They are a class of solutions reduce to ODEs, granted the assumption of polynomial initial bubble shapes, until the ordinary differential equations are integrated in time. They are primarily analytical solutions which are reliable for comparison with fully numerical solutions.

3.3.2 A Non-collapsing Bubble in Pure Straining Flow

For analytical solutions, changes in the problem dynamics, such as the type of far-field flow or the initial bubble shape, are not trivial. Rather than merely changing the values of a couple parameters it is often the case that the evolution equations must be derived afresh from (3.44, 3.45). Below, we discuss the derivation of evolution equations for a bubble placed in a pure straining flow following [26] with several corrections.

Pure straining flow is given by setting the far-field parameters (2.9) $\alpha_0 = Q$ and $\beta_0 = \omega_0 = 0$. Consequently, the far-field velocity is

$$\mathbf{u}_\infty = (Cx, -Cy), \tag{3.54}$$

where C is the capillary number

$$C = \frac{Q\mu L}{\sigma_0}. \tag{3.55}$$

The appearance of the capillary number in the far-field flow is determined by the non-dimensionalization of $\mathbf{u}_\infty$ (2.9). Physically, pure straining flow is similar to a flow driven by Taylor's four-roller mill [24, 27], in which a bubble placed in the center will stretch along the horizontal axis and compress along the vertical axis (see figure (3.3)).

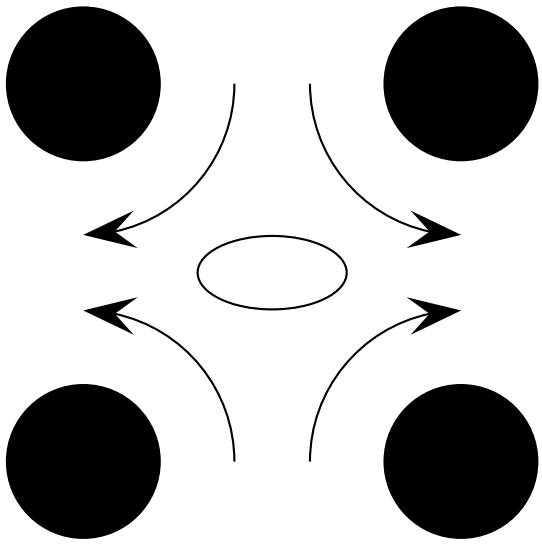

Figure 3.3: Taylor's four-roller mill.

We consider elliptical bubbles. This corresponds to $N = 1$ in (3.46):

$$z(\zeta, t) = a(t)/\zeta + b(t)\zeta. \tag{3.56}$$

The coefficients a and b are assumed real. The analysis provided in [26] indicates that for later times, the bubble will maintain a profile of this form. From the ODEs (3.45), we find that the evolution of a bubble in pure straining flow is given by

$$\frac{\mathrm{d}(ab)}{\mathrm{d}t} = -2I_0 ab + Ca^2. \tag{3.57}$$

We assume that the bubble area remains constant so that (3.44) provides the area condition,

$$a^2 - b^2 = R^2. \tag{3.58}$$

Here, R is the radius of the initial bubble, which we assume is a circle. In general we choose $R = 1$, but leave it here for completeness. To compute I_0, we set $N = 1$ in (3.49),

$$\begin{aligned} I_0(a,b) &= \frac{1}{2\pi}\int_0^\pi \frac{d\nu}{\{a^2+b^2-2ab\cos(\nu)\}^{1/2}} \\ &= \frac{1}{\pi|a|}\frac{1}{\rho+1}K\left[\frac{4\rho}{(1+\rho)^2}\right]. \end{aligned} \tag{3.59}$$

It is convenient to define the parameter $\rho = b/a$. From the area condition it is possible to express a and b in terms of ρ. Observe,

$$\begin{aligned} 1 - b^2/a^2 &= R^2/a^2 \\ 1 - \rho^2 &= R^2/a^2 \end{aligned}$$

so that

$$\begin{aligned} a^2 &= \frac{R^2}{1-\rho^2} \\ b &= \rho a. \end{aligned} \tag{3.60}$$

Dividing (3.57) by the product ab, we have

$$\begin{aligned} \frac{(ab)_t}{ab} &= \frac{a_t b}{ab_t} = -2I_0 + C\frac{a}{b} \\ &= \frac{a_t}{a} + \frac{b_t}{b} = -2I_0 + \frac{C}{\rho}. \end{aligned} \tag{3.61}$$

We may calculate the terms on the left hand side by appealing to the area condition and the definition of ρ:

$$\begin{aligned} \frac{a_t}{a} &= \frac{\rho\dot{\rho}}{(1-\rho^2)} \\ \frac{b_t}{b} &= \frac{\dot{\rho}}{\rho} + \frac{\rho\dot{\rho}}{(1-\rho^2)}. \end{aligned}$$

We can make these substitutions to obtain an evolution ODE in ρ:

$$\dot{\rho} = \frac{1-\rho^2}{1+\rho^2}(C - 2\rho I_0). \tag{3.62}$$

Tanveer and Vasconcelos [26] report that steady-state solutions only exist for capillary numbers below a certain critical value; $0 < C < C_{crit} = 0.6097$. In figure (3.4) we present a steady-state solution obtained for capillary number $C = 0.5$. The capillary number captures the speed of the far-field flow, and can be intuitively associated with the strain rate Q.

For contrast we also present an unsteady solution with $C = 0.7$. This corresponds to an increase in the strain rate. Stretching along the horizontal axis continues without approaching a steady-state. Integration beyond the final time $t = 12$ failed, however, as the elliptic integral blows up (similarly to the previous example). This time may represent the point at which a bubble bursts. Such a conjecture seems to be supported by Buckmaster and Flaherty [4] who argue that certain parameter values for which steady-state solutions do not exist correspond to bubble bursting.

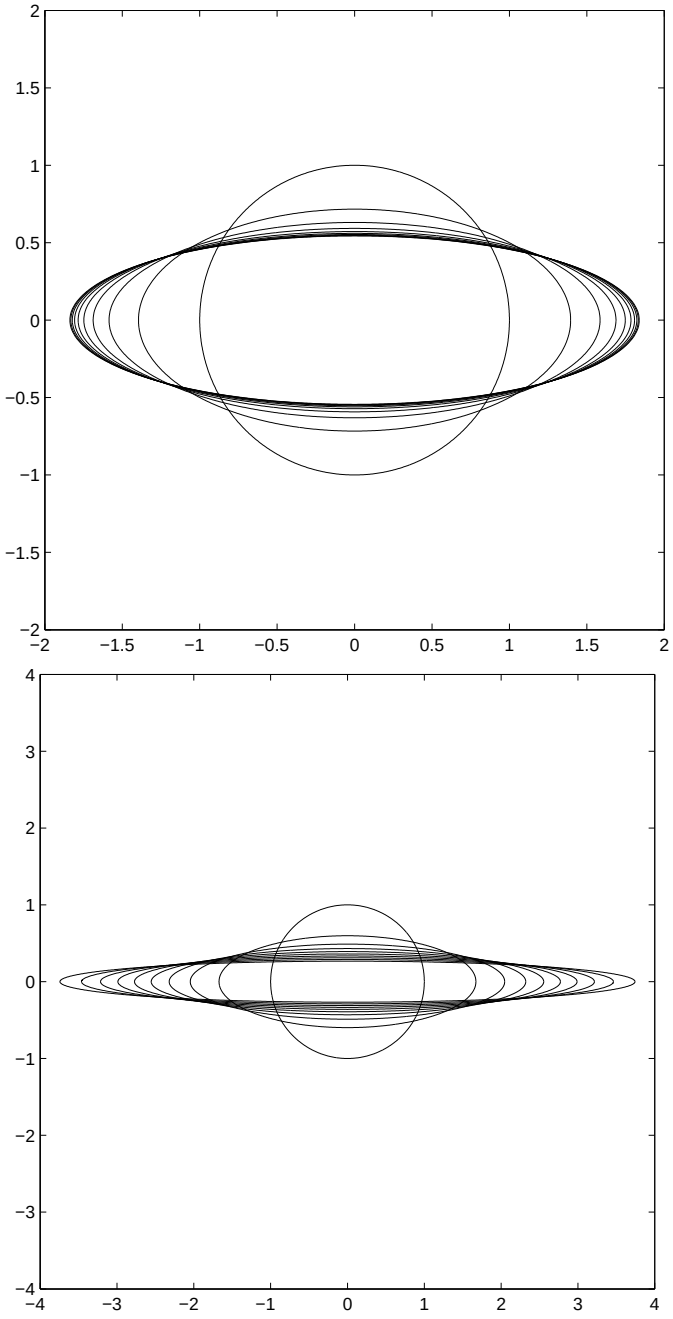

Figure 3.4: On the top, a circular bubble with initial parameters $a(0) = 1$, $b(0) = 0$, capillary number $C = 0.5$, and area $A = \pi$ placed in a pure straining flow approaches steady-state. On the bottom, $C = 0.7$; an unsteady solution. The bubble evolves until $t = 12$.

Chapter 4

Surfactant and Analytical Solutions

As discussed in section (2.4), the inclusion of surfactant has the effect of introducing a variable surface tension into the boundary conditions on the fluid-bubble interface. In this chapter we investigate analytical solutions to bubbles with surfactant. The analysis followed here has been outlined by Siegel [23]. Like the *clean-flow* (no surfactant) solutions in chapter (3), these solutions neglect the effects of gravity resulting in a zero Bond number.

4.1 Modified Analytical Solutions

Much of the analysis employed in finding clean-flow solutions carries over here. Solving the Stokes equations in two-dimensions is equivalent to solving the scalar biharmonic equation (3.3) by introducing a stream function (3.2). According to the Goursat representation for biharmonic functions, the stream function can be expressed in terms of complex analytic functions (3.17). All relevant physical quantities can likewise be expressed in terms of the analytic functions (3.18, 3.19, 3.20). We find the analytic functions by imposing boundary conditions on them. The far-field conditions are given in (3.21, 3.22).

The interface condition, however, is modified by the spatially varying surface tension as a result of the presence of surfactant. We follow this step carefully since it is here that these solutions differ from the clean-flow solutions. From (2.14), we have

$$-p\mathbf{n} + 2\mathbf{E}\cdot\mathbf{n} = -\sigma\kappa\mathbf{n} + \nabla_s\sigma. \tag{4.1}$$

Recalling (3.25) and the definitions of the unit normal (3.23) and curvature (3.26) we can

rewrite this condition in terms of the Goursat functions. We follow [23] in doing so.

$$\begin{aligned} -2(\phi - z\overline{\phi'} - \overline{\psi})_s &= \sigma\kappa i z_s + \sigma_s z_s \\ &= \sigma z_{ss} + \sigma_s z_s \\ &= (\sigma z_s)_s \end{aligned} \tag{4.2}$$

Combining the two terms involving σ as above consolidates the influence of surface tension in one term. By tracking this term, we find that the original analytical solution is relatively unchanged. Indeed, surface tension influences only one term in the solution and we may retain much of the analysis. To see this, integrate both sides by s to find

$$\phi - z\overline{\phi'} - \overline{\psi} = -\frac{\sigma(s,t)z_s}{2}. \tag{4.3}$$

In terms of velocity, the interface condition is

$$u + iv = -i\frac{\sigma(s,t)z_s}{2} - 2i\phi. \tag{4.4}$$

Combining the stress interface condition with the kinematic condition (3.32), the resulting condition is

$$\mathrm{Re}\left(\frac{z_t + 2i\Phi(\zeta,t)}{\zeta z_\zeta}\right) = \frac{\sigma(s,t)}{2|z_\zeta|}. \tag{4.5}$$

At this stage we must appeal to Poisson's formula, as discussed in section (3.2). The right hand side of (4.5) provides the boundary data for Poisson's formula. Extended into the unit circle of the ζ-domain, we now have

$$z_t + 2i\Phi(\zeta,t) = \zeta[I(\zeta,t) + iC]z_\zeta, \tag{4.6}$$

where

$$I(\zeta,t) = \frac{1}{4\pi i}\oint_{|\zeta'|=1} \frac{\sigma(\zeta',t)}{|z_\zeta(\zeta',t)|}\left[\frac{\zeta'+\zeta}{\zeta'-\zeta}\right]\frac{d\zeta'}{\zeta'}. \tag{4.7}$$

In computing solutions, we make almost exclusive use of the first term in a Taylor expansion of $I(\zeta,t)$. This is incidental to the examples studied here, and not to any truncation of terms.

Similar to (3.42), this term is

$$I_0 = \frac{1}{4\pi}\int_0^{2\pi} \frac{\sigma(\nu,t)}{|z_\zeta(e^{i\nu},t)|}d\nu. \tag{4.8}$$

Compare $I(\zeta,t)$ to (3.33) and observe that the only difference with the clean flow problem is the addition of a variable $\sigma(\nu,t)$ (The constant *sigma* was removed by non-dimensionalizing). This is the only point at which surfactant has an effect on analytical solutions. The system of ordinary differential equations (3.44, 3.45) remains unchanged in the surfactant case. Only computations of $I(\zeta,t)$ need to be modified.

4.2 Surfactant Transport in Complex Variables

As the interface boundary condition is affected by surface tension, so also does surface tension depend on the non-uniform distribution of surfactant concentration. Surfactant concentration is transported along the fluid-bubble interface according to the surfactant transport equation in (2.26). Here we rewrite the transport equation in terms of complex variables consistent with our analytical solutions.

The spatial variable is no longer arclength (s) but ν, the parameter that describes movement along the unit circle in the ζ-plane defined in (3.42). Spatial derivatives are equated by the relation

$$\frac{\partial}{\partial s} = \frac{1}{|z_\nu|}\frac{\partial}{\partial \nu}. \tag{4.9}$$

This can be thought of as the chain rule where $|z_\nu|$ is likened to the change in arclength with respect to ν. The unit tangent and normal vectors are given by

$$\mathbf{s} = \frac{z_\nu}{|z_\nu|} \tag{4.10}$$

$$\mathbf{n} = -i\mathbf{s} = -i\frac{z_\nu}{|z_\nu|}, \tag{4.11}$$

which is consistent with our previous definition in terms of θ (3.23).

The first term of (2.26), the partial time-derivative of surfactant concentration, is unchanged.

The second term:

$$\begin{aligned}\frac{\partial \mathbf{x}}{\partial t}\cdot\nabla_s\Lambda &= z_t\cdot\mathbf{s}\frac{\partial\Lambda}{\partial s}\\ &= z_t\cdot\frac{1}{|z_\nu|}\Lambda_\nu\frac{z_\nu}{|z_\nu|}\\ &= \mathrm{Re}\left(z_t\Lambda_\nu\frac{\bar{z}_\nu}{|z_\nu|^2}\right)\\ &= \mathrm{Re}\left(\frac{z_t\Lambda_\nu}{z_\nu}\right).\end{aligned} \tag{4.12}$$

The last step is accomplished with the identity $z_\nu\bar{z}_\nu = |z_\nu|^2$.

The third term:

$$\begin{aligned}\nabla_s\cdot(\Lambda\mathbf{u}) &= \mathbf{s}\frac{\partial}{\partial s}\cdot\Lambda\mathbf{u}\\ &= \frac{\partial}{\partial s}(\mathbf{s}\cdot\Lambda\mathbf{u})\\ &= \frac{1}{|z_\nu|}\frac{\partial}{\partial\nu}\mathrm{Re}\left(\frac{\bar{z}_\nu}{|z_\nu|}\Lambda\mathbf{u}\right)\\ &= \frac{1}{|z_\nu|}\frac{\partial}{\partial\nu}\mathrm{Re}(P).\end{aligned} \tag{4.13}$$

where,

$$P(\nu,t) = \frac{\mathbf{u}\bar{z}_\nu\Lambda}{|z_\nu|}. \tag{4.14}$$

In the fourth term, the surface divergence of the unit normal vector appears. It can be related to curvature (3.26) by

$$\begin{aligned}\nabla_s\cdot\mathbf{n} &= \mathbf{s}\cdot\frac{\partial\mathbf{n}}{\partial s}\\ &= \mathbf{s}\cdot(-ie^{i\theta})_\theta\theta_s\\ &= \mathbf{s}\cdot(e^{i\theta})\theta_s\\ &= \mathbf{s}\cdot\mathbf{s}\kappa\\ &= \kappa,\end{aligned} \tag{4.15}$$

where we have also made use of the definition of the unit normal vector (3.23). Curvature

can in term be expressed in terms of complex variables. From the definition of curvature given in [13],

$$\begin{aligned}
\kappa &= \frac{(x_\nu y_{\nu\nu} - x_{\nu\nu} y_\nu)}{|z_\nu|^3} \\
&= \tfrac{1}{|z_\nu|^3}(x_\nu, -y_\nu) \cdot (y_{\nu\nu}, x_{\nu\nu}) \\
&= \tfrac{1}{|z_\nu|^3}\bar{z}_\nu \cdot i\bar{z}_{\nu\nu} \\
&= \tfrac{1}{|z_\nu|^3}\mathrm{Re}(\bar{z}_\nu(-i)z_{\nu\nu}) \\
&= \tfrac{1}{|z_\nu|^3}\mathrm{Im}(\bar{z}_\nu z_{\nu\nu}) \\
&= \tfrac{1}{|z_\nu|}\mathrm{Im}(\frac{\bar{z}_\nu}{|z_\nu|^2} z_{\nu\nu}) \\
&= \frac{1}{|z_\nu|}\mathrm{Im}(\frac{z_{\nu\nu}}{z_\nu}) \qquad (4.16)
\end{aligned}$$

The fourth term:

$$\begin{aligned}
\Lambda(\nabla_s \cdot \mathbf{n})(\mathbf{u} \cdot \mathbf{n}) &= \Lambda\kappa \mathbf{u} \cdot \mathbf{n} \\
&= \Lambda\kappa \mathrm{Re}\left(\mathbf{u}\left(\overline{-i\frac{z_\nu}{|z_\nu|}}\right)\right) \\
&= -\Lambda\kappa \mathrm{Im}\left(\mathbf{u}\frac{\bar{z}_\nu}{|z_\nu|}\right) \\
&= -\kappa \mathrm{Im}(P). \qquad (4.17) \\
&= -\frac{1}{|z_\nu|}\mathrm{Im}(\frac{z_{\nu\nu}}{z_\nu})\mathrm{Im}(P) \qquad (4.18)
\end{aligned}$$

The fifth term:

$$\begin{aligned}
\frac{1}{Pe_s}\nabla_s^2 \Lambda &= \frac{1}{Pe_s}\mathbf{s}\frac{\partial}{\partial s} \cdot \left(\mathbf{s}\frac{\partial}{\partial s}\Lambda\right) \\
&= \frac{1}{Pe_s|z_\nu|}\frac{\partial}{\partial \nu}\left(\frac{\Lambda_\nu}{|z_\nu|}\right) \qquad (4.19)
\end{aligned}$$

The complete transport equation for Λ is

$$\frac{\partial \Lambda}{\partial t} = \mathrm{Re}\left(\frac{z_t \Lambda_\nu}{z_\nu}\right) - \frac{1}{|z_\nu|}\frac{\partial}{\partial \nu}\mathrm{Re}(P) + \frac{1}{|z_\nu|}\mathrm{Im}(\frac{z_{\nu\nu}}{z_\nu})\mathrm{Im}(P) + \frac{1}{Pe_s|z_\nu|}\frac{\partial}{\partial \nu}\left(\frac{\Lambda_\nu}{|z_\nu|}\right). \qquad (4.20)$$

At each time step, the velocity on the boundary ($\mathbf{u}$) must be computed. Using (4.4) to

eliminate $\Phi(\zeta, t)$ from (4.6) we obtain an expression for velocity (see [23]),

$$z_t - \mathbf{u} = \zeta z_\zeta \left[\frac{1}{4\pi i} PV \int_0^{2\pi} \frac{\sigma(\nu', t)}{|z_\nu(\nu', t)|} \cot \frac{\nu' - \nu}{2} d\nu' \right], \tag{4.21}$$

where PV denotes Cauchy principal value integral. In [15], Kropinski shows that such an integral can be solved using the Hilbert transform. The new expression for $\mathbf{u}$ is

$$\mathbf{u} = z_t - \zeta z_\zeta \left[-\frac{1}{2i} \mathcal{H} \left(\frac{\sigma}{|z_\nu|} \right) \right], \tag{4.22}$$

where the $\mathcal{H}$ is the Hilbert transform [19], which can be computed in Fourier space by

$$\mathcal{H}(e^{inx}) = -i \ \mathrm{sgn}(n) e^{inx}, \quad \mathcal{H}(1) = 0. \tag{4.23}$$

The function $\mathrm{sgn}(n)$ denotes the sign function.

4.3 Computed Solutions

Computing solutions to a time-evolving surfactant-laden bubble requires solving the surfactant transport equation (4.20) coupled with the ODEs characterizing evolution of the bubble interface (3.44, 3.45). The influence of surfactant on the evolution of a bubble is concentrated in computing I_0 (4.8).

A pseudo-spectral method is employed to compute surfactant transport. Simply stated, the spatial derivatives are computed using Fast Fourier Transforms (FFTs), leaving ODEs in time which may be computed using some other method (e.g. Runge-Kutta). By contrast a (fully) spectral method computes even the time-derivatives in Fourier space, and thus evolves Fourier coefficients ($\hat{\Lambda}$) rather than the function itself (Λ).

Pseudo-spectral methods are a natural choice for this problem. First, by representing the surfactant distribution in Fourier space, computing spatial derivatives is reduced to multiplication. These computations are spectrally accurate, meaning convergence is exponential. They can therefore be used to produce highly accurate computations. Second, the periodicity of the bubble interface, and hence the domain of surfactant concentration is amenable to FFTs.

Surfactant concentration is expressed below as a sum of its Fourier coefficients, followed by its derivatives. The interface of the bubble is discretized into N marker points, given by

ν_j, where $0 \leq j \leq N$. Derivatives are given at the marker points.

$$
\begin{aligned}
[\Lambda]_j &= \sum_{k=-N/2}^{N/2-1} \hat{\Lambda}_k e^{ik\nu_j}, \\
[\Lambda_\nu]_j &= \sum_{k=-N/2}^{N/2-1} ik\hat{\Lambda}_k e^{ik\nu_j}, \\
[\Lambda_{\nu\nu}]_j &= \sum_{k=-N/2}^{N/2-1} -k^2\hat{\Lambda}_k e^{ik\nu_j}.
\end{aligned} \tag{4.24}
$$

Derivatives of z and P may be similarly computed.

There are limitations to pseudo-spectral methods. First, using multiple forward and backward transforms at each time step can become very costly timewise. In this regard, spectral methods may be preferable since backward transforms may be eliminated from the inner loop. Second, accuracy is lost when a function cannot be easily represented with a Fourier series.

After computing spatial derivatives spectrally, the coupled problem is reduced to a set of ODEs. We compute them using a second order Runge-Kutta method (modified Euler) [5]. 2nd order convergence has been verified by numerical experiments. Because of the small time-steps required by the stability constraint, truncation errors are sufficiently small. A higher order method could be implemented for computing to the desired accuracy. It would have been advantageous to compute the highest derivatives (e.g. the diffusion term) implicitly, but $|z_\nu|$ is not known in advance and is computed explicitly. [1]

Solutions to these ODEs are computed in FORTRAN. It is preferable to computing in MATLAB because of computational speed. Computational time for bubble simulations range between 10 mins and 48 hrs. All computations cited were performed on a Compaq Alpha ES-40.

Mesh adaption is employed. When the surfactant concentration becomes under-resolved, the number of marker points is doubled and the time step is divided by 4 according to the

[1] $|z_\nu|$ is constant and may be known in advance, however, when marker points are equally spaced along the interface [13]. It is also possible to compute $|z_\nu|$ explicitly and still use an implicit method [7].

stability constraint:

$$\frac{\Delta t}{(\Delta\nu)^2} \leq C. \tag{4.25}$$

The resolution is determined inadequate when the magnitude of any Fourier coefficient in the upper or lower quarters of the Fourier spectrum exceeds 10^{-12}. When the number of marker points doubles, the Fourier spectrum is padded with zeros. When the inverse FFT is applied, the new grid points are assigned values automatically (according to Fourier interpolation).

Since no surfactant is added to or leaves the interface of the bubble, total surfactant should be conserved for all time. Total surfactant [23] may be calculated by

$$T = \int_0^{2\pi} \Gamma |z_\nu| d\nu. \tag{4.26}$$

This is a helpful test of computational accuracy. Throughout a bubble simulation in FORTRAN, total surfactant only changed a fraction of a percent. The code was also tested by setting $\beta = 0$ (surfactant has no influence on bubble evolution; see equation (2.15)) and reproducing the clean-flow solutions.

Plots of surfactant concentration, bubble profile, and the Fourier spectrum of Λ are output and we present the results of several simulations below.

4.3.1 Collapsing Bubbles

We return to our experiments with collapsing bubbles, introduced in section (3.3.1), in order to compare evolving bubbles with surfactant to those without. Collapsing bubbles are not the easiest examples with which to begin. Several experiments were performed on simpler stationary ellipses with non-uniform surfactant distributions. One distribution used, that of a Gaussian having only one concentrated area of non-uniformity, should have made the effects of surfactant obvious. Unfortunately, it proved difficult to resolve the Gaussian adequately with a limited number of marker points. More readily resolved patterns were experimented with as well, but unfortunately they were too un-featured to produce any noticeable changes in the evolution of a bubble. This was compounded by the lack of exterior fluid velocity.

The profile of a collapsing bubble, however, is noticeably modified by the presence of

surfactant. We set the surface Peclet number $Pe_s = 1000$ in order to suppress diffusion for all simulations with the exception of the second simulation. (For small values of Pe_s, features in the surfactant profile can be difficult to detect.) While analyzing the results, it became apparent that all of these simulations either break symmetry constraints on Λ or produce non-physical solutions in some other way. Nevertheless, they are more interesting than correct solutions because they illustrate why certain solutions do not work.

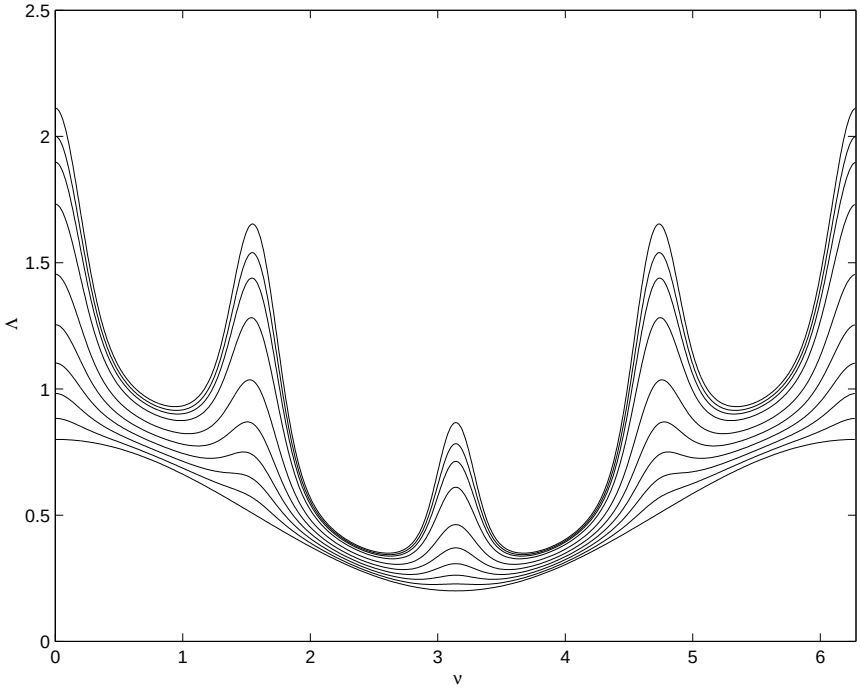

Figure 4.1: Simulation 1: Evolution of surfactant concentration on a collapsing four-fold symmetric bubble. The topmost profile is at $t = 0.28$.

Simulation 1

Figure (4.1) displays the evolution of the surfactant profile for a simple initial distribution. The initial distribution is the lowest profile in figure and is given by the function

$$\Lambda_0 = \tfrac{3}{5}\cos^2(\nu/2) + \tfrac{1}{5}. \tag{4.27}$$

On the right side of the bubble sits the bulk of surfactant and on the left side it is spread thinly. We set $\beta = 0.5$, the other parameters as in figure (3.1), and evolve until $t = 0.28$. Surfactant concentration is plotted against $\nu = 0$ to 2π, which increases in the clockwise direction (see figure (2.1) for orientation).

The progression of surfactant profiles indicates that the concentration of surfactant increases everywhere along the interface. As the bubble contracts, the length of the interface decreases. Because surfactant is conserved on the bubble, there is more surfactant per unit of interface. The other prominent feature is that the surfactant is drawn out in four equally spaced spikes. The contraction of the bubble is a mechanism for convecting surfactant to the four corners, as cusps form. According to the linear equation of state (2.15), the surface tension is lowest at these local maxima.

Figure (4.2) displays the corresponding bubble profile, and that of a bubble without surfactant evolved to the same time. The profiles become more frequent on the left when the mesh is adapted and the time step decreases. The differences are subtle, but differences in curvature along the inner bubble are noticeable. Using the formula for maximum curvature (3.53) we find that for the surfactant-laden bubble, $\kappa^* = 38.7937$ whereas for the clean bubble, $\kappa^* = 19.1912$. The development of a cusp is therefore accelerated by the presence of surfactant.

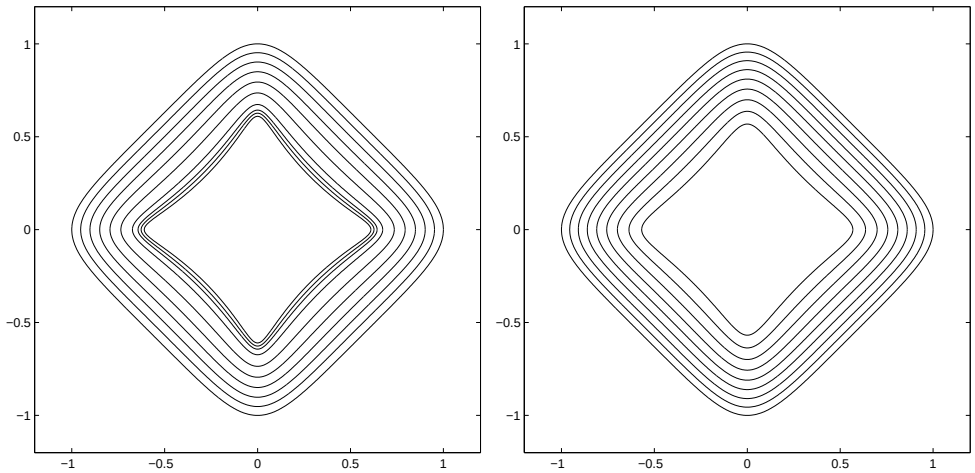

Figure 4.2: Collapsing four-fold symmetric bubbles. On the left, a surfactant laden bubble with $\beta = 0.5$ (simulation 1). On the right, a clean bubble. The inner profiles are at $t = 0.28$.

We also expect to see a difference between the left and right sides because of the uneven surfactant distribution, but instead they look very similar. It may be the case that a simple two-parameter (a and b) polynomial representation of a bubble cannot account for the differences in surfactant distribution on the left and right sides. In other words, two parameters are not be enough to capture the detail introduced by a general surfactant distribution. It seems the bubble is required to maintain four-fold symmetry and thus should not respond to differences in surfactant from one quadrant to the next.

Simulation 2

With this in mind, the choice of Λ_0 in the second simulation is made to cause the distribution of surfactant in each of the four quadrants to conspire. If Λ_0 is four-fold symmetric, hopefully the effects of surfactant will be evident in each of the four quadrants. Figure (4.3) displays the evolution of a four-fold symmetric distribution of surfactant given by the function

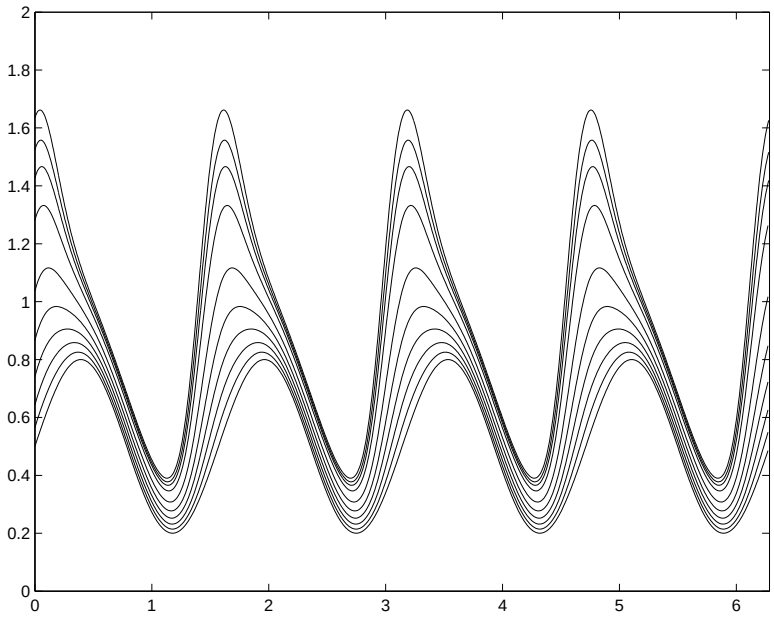

Figure 4.3: Simulation 2: Evolution of surfactant concentration. The topmost profile is at $t = 0.28$.

The crests of Λ_0 do not coincide with the four corners of the bubble. This was done to maximize the gradient of surfactant, and hence the Marangoni forces (see equation (2.14)),

where cusps form. In retrospect, however, it is the concentration itself and not the gradient that influences the bubble evolution through I_0. The parameters are the same as for the first collapsing bubble simulation in figures (4.1, 4.2) with the exception of $Pe_s = 100$ and the final profile is at $t = 0.28$.

$$\Lambda_0 = \tfrac{3}{5}\cos^2(2\nu - \pi/4) + \tfrac{1}{5}. \tag{4.28}$$

We see that surfactant concentration maintains four-fold rotational symmetry throughout the duration of the simulation, but reflective symmetry is lost. For this reason, the accuracy of this solution is also in doubt. Siegel [23] imposes a two-fold symmetry constraint when studying elliptical ($N = 1$) bubbles, which seems to suggest that four-fold rotational and reflective symmetry is required when $N = 3$. Further investigation is required to understand the precise nature of symmetry restrictions on Λ.

The maximum curvature on the inner bubble is $\kappa^* = 38.162$, which is slightly less than the maximum curvature in the first simulation. Comparing surfactant in the two simulations, we see that the surfactant concentration is greater on three of the four spikes in the first simulation. This has the effect of creating a lower surface tension, which explains why the maximum curvature is higher. In fact, the surfactant concentration is so high on the right spike that surface tension is negative at this point.

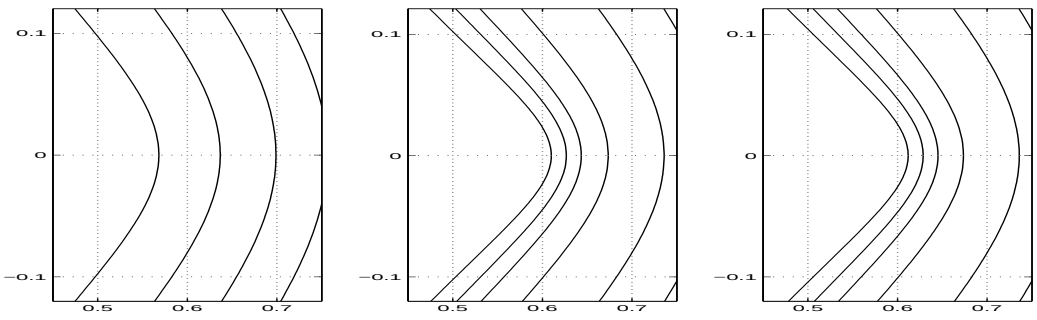

Figure 4.4: Close up comparison from left to right: A clean bubble, simulation 1, and simulation 2. The innermost profiles are at $t = 0.28$.

A close up plot of the innermost bubble profile appears in figure (4.4), compared with a clean bubble and simulation 1. Increased curvature can be observed on bubbles with surfactant. Another notable feature is the advancement of the inner profile. On the bubbles

with surfactant, the profile is less advanced where the cusp forms.

Simulation 3

Neither of the previous simulations test the limits of computability, but the third simulation is directed at computing a collapsing surfactant-laden bubble as far as possible. The same parameters are chosen as in the previous simulations, $Pe_s = 1000$, and the idealistic final time is set to 0.356. This is the time to which a collapsing bubble without surfactant is computed in [15], and if successful, would have made an interesting case for comparison [2]. The choice of Λ_0 is a simple variation on those previously chosen:

$$\Lambda_0 = \tfrac{3}{5}\cos^2(3\nu/2 - \pi/4) + \tfrac{3}{5}. \tag{4.29}$$

The simulation ran for approximately 48 hours and then ceased due to numerical overflow, computing to $t = 0.339$. A ceiling of allowable marker points was set at 32768. When this number of marker points failed to accurately resolve surfactant concentration, the number of marker points could not be increased and the higher frequency Fourier modes grew unbounded. Fortunately, the data from the simulation was preserved until shortly before overflow. The evolution of surfactant concentration appears in figure (4.5).

Because Λ_0 does not share the periodicity of the four-fold bubble, four interesting non-uniform spikes emerge. The length of the simulation causes the surfactant concentration to exceed 2.5; significantly more than the concentration levels in the previous simulations. The space between plots becomes less and less as the marker points and time steps are modified in mesh adaption. The dynamics at the tops of the spikes requires closer examination and the fourth spike is enlarged in figure (4.6).

From the plot densities, we can see that the spike grows up to a peak near $\Lambda = 2.7$, and then shrinks back to $\Lambda = 2.6$ where it begins to split into two lesser peaks. The phenomena of retreating spikes was not observed in previous simulations. It is the subject of curiosity, requiring some explanation. As noted in simulation 2, for $\beta = 0.5$ the surface tension of the bubble becomes negative when $\Lambda = 2$. Negative surface tension is non-physical and may have undesirable side-effects. It is likely such effects were not present in simulation 2 because negative surface tension in a few regions was balanced by the positive surface tension everywhere else. Local surface tension has a global influence through through I_0. Simulation

[2] It should be noted that [15] does not report reaching a limit at $t = 0.356$.

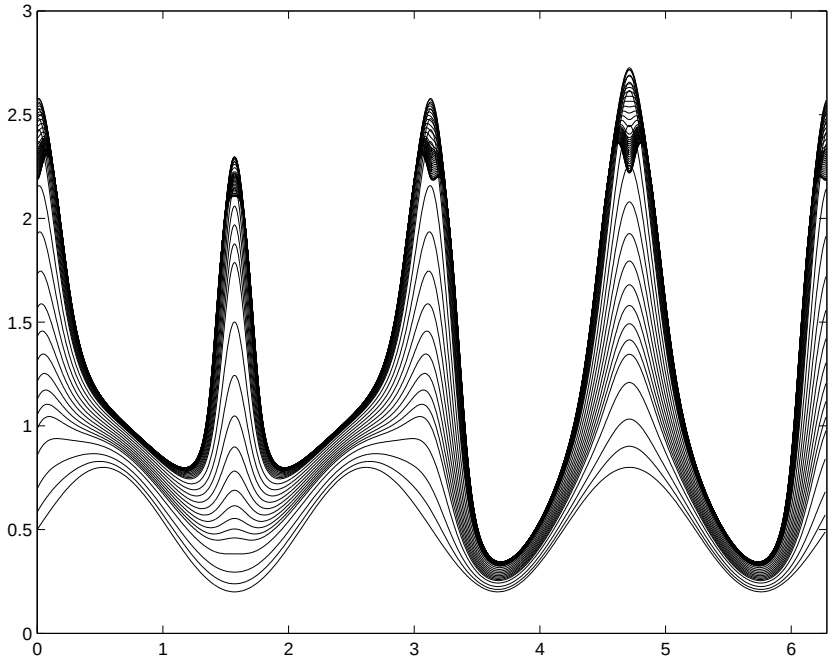

Figure 4.5: Simulation 3: Evolution of surfactant concentration until $t = 0.339$.

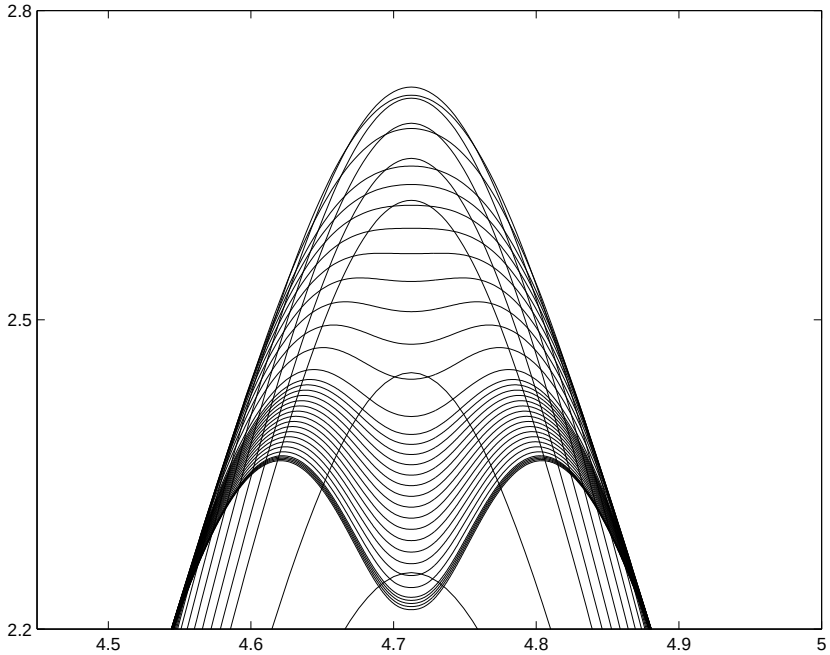

Figure 4.6: Magnification of the fourth spike in figure (4.5)

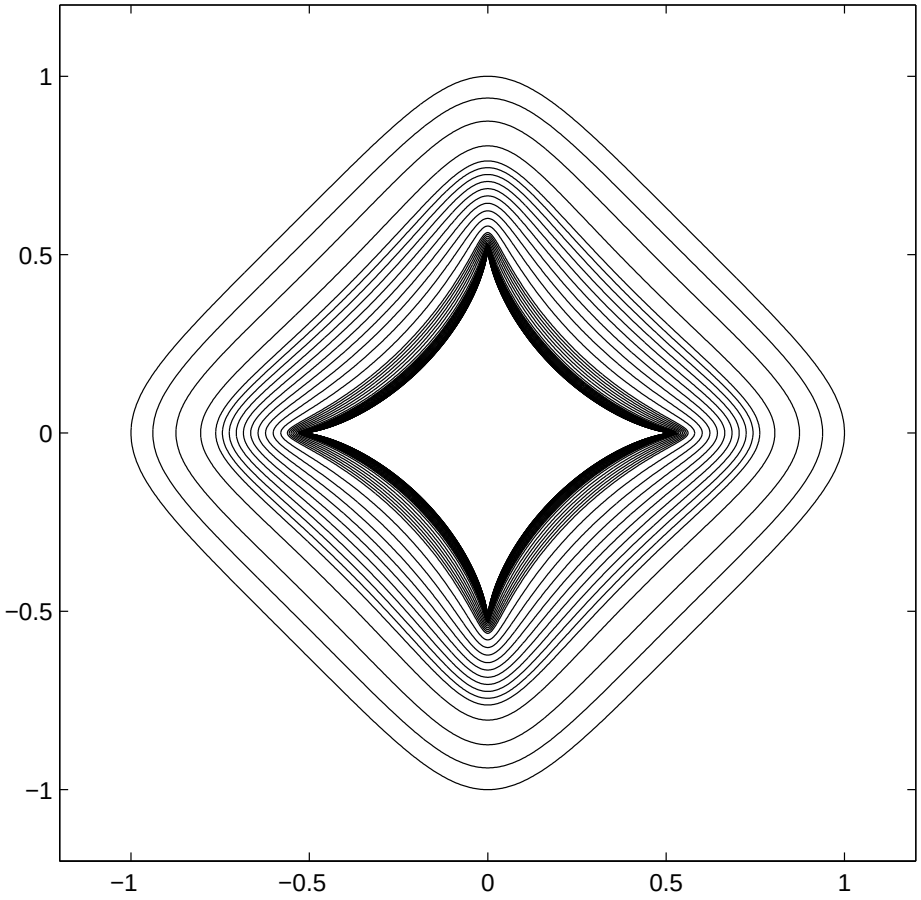

Figure 4.7: Simulation 3: A bubble collapses until $t = 0.339$.

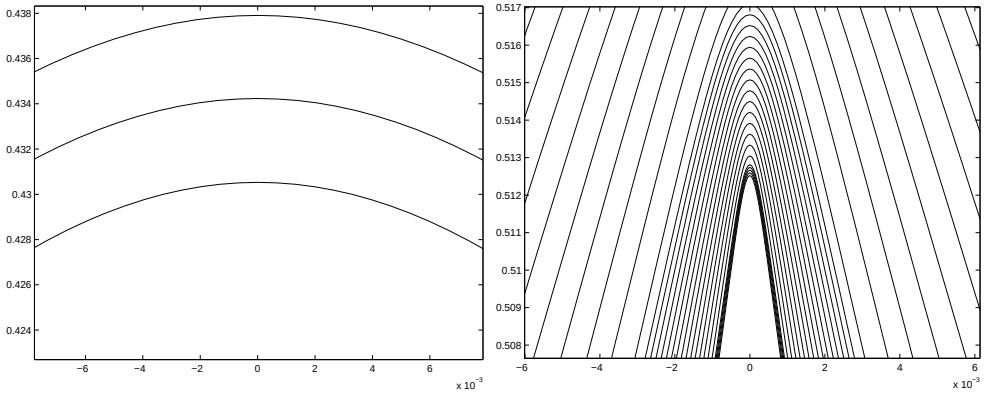

Figure 4.8: Close up comparison: a clean bubble, and simulation 3 (4.7)

3, however, provides a sufficient amount of time for the effects of negative surface tension to compound and conspire. It seems that the retreating spike is caused by negative surface tension. Examining the transport equation (4.20), we see that surface tension influences surfactant transport through $P(\nu, t)$.

The retreating spike may also indicate a weakness in the linear equation of state chosen (2.15). Siegel [23] uses this equation of state only for small β values, which reduces the risk of getting negative surface tension. Alternatively, more complicated equations of state may be employed; e.g. quadratic or cubic functions for surface tension.

The bubble profiles (figure (4.7)), on the other hand, do not indicate any outward retreat, as with surfactant. They continue collapsing steadily and do not double back, even though the influence of negative surface tension is evident. Nevertheless, cusp formation is advanced when compared with a clean bubble at the same time (figure (4.8)). The maximum curvature on the inner bubble in simulation 3 is $\kappa^* = 3.0601 \times 10^4$ compared to $\kappa^* = 9.8337 \times 10^2$ on a clean bubble at the same time; a remarkable increase.

4.3.2 Pure Straining Flow

The experiments with pure straining flow are a rather anticlimactic finale to this study. The computational duration of these simulations approaching steady-state made it difficult to explore computational limitations. Nonetheless, they seem to be the most reliable in terms of avoiding non-physical solutions and respecting symmetry constraints. One experiment is reported here.

The initial distribution of surfactant, Λ_0, is chosen to be uniformly equal to 1. We set the Capillary number (modestly) to $C = 0.2$, the parameters $a(0) = 1$, $b(0) = 1$ (initial bubble a unit circle), and evolve until $t = 2$. The evolution of surfactant concentration appears in (4.9). Surfactant is transported along the major axis of the bubble and collects at the ends. The average surfactant concentration around the bubble interface remains 1 for all time, since the bubble area does not change.

By performing an analytical steady-state calculation, Siegel [23] reports that eventually regions of the bubble will be swept clean of surfactant, leaving "surfactant caps" on the ends. As the capillary number increases, the bald region of the bubble grows until a critical value where a steady-state may no longer be possible. Siegel's results indicate that one would need to compute to $t = 64$ to see a surfactant cap with these parameters. It was the hope of the present author to compute surfactant caps in a time-dependent simulation,

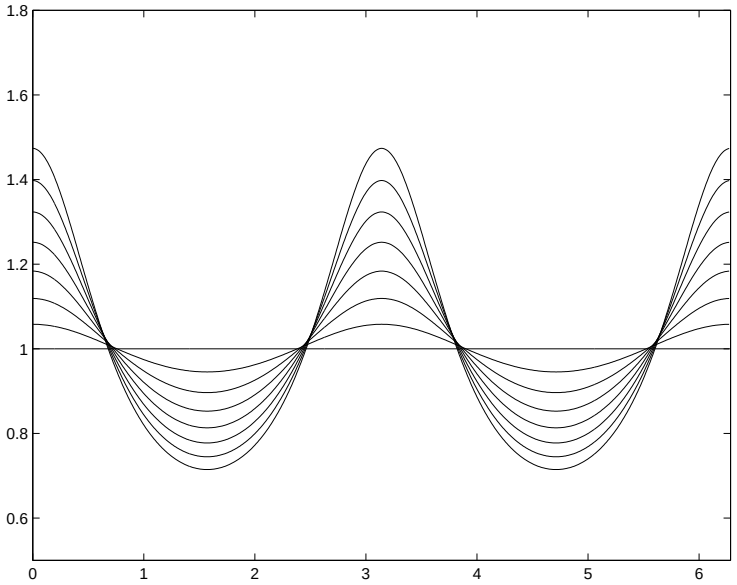

Figure 4.9: Pure Strain: Evolution of surfactant concentration. Final profile at $t = 2$.

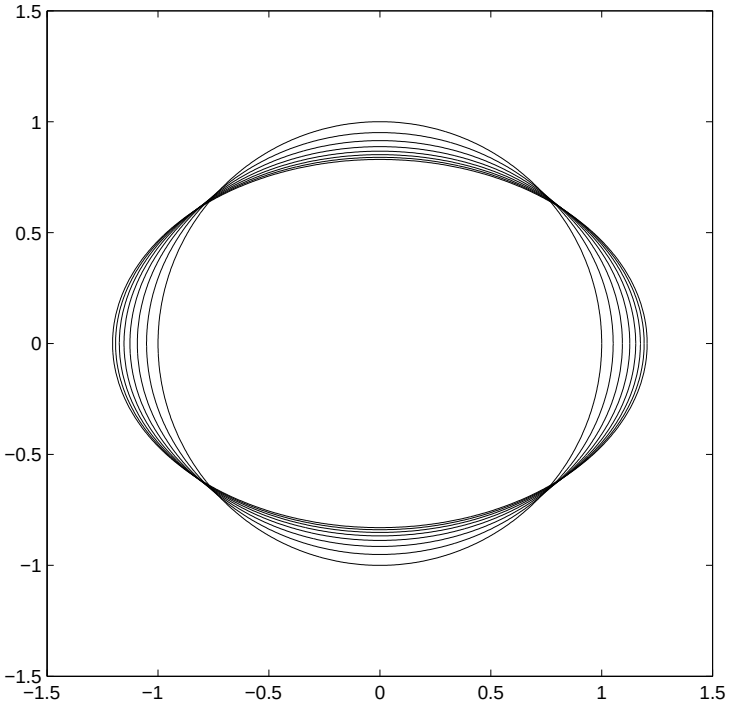

Figure 4.10: Pure Strain: Evolution of an initially circular bubble. Final profile at $t = 2$.

but unfortunately it proved too expensive. It took approximately 48 hours to compute to $t = 6.8$, where the simulation became very slow due to mesh refinement. An alternative computational approach is required to compute surfactant caps.

The evolution of the bubble (4.10) indicates that it, unlike the surfactant concentration, is rapidly approaching a steady-state. We also find that its behavior in the presence of surfactant is comparable to that in previous simulations. The maximum curvature is $\kappa^* = 1.7495$, compared to $\kappa^* = 1.6837$ on a clean bubble evolved to the same time. In addition, the bubble is more deformed in the presence of surfactant. The right end of the bubble extends to $x = 1.205$, compared to $x = 1.19$ on a clean bubble.

Cusp formation is possible in a pure straining flow. Using an expression for far-field flow with cubic terms, Siegel [23] obtains a steady-state result with cusps. Cusp formation does not, however, appear to be possible with the current far-field flow.

Chapter 5

Conclusion

We have investigated computational solutions to evolving surfactant-laden bubbles in slow viscous flow. In particular, we computed solutions to a collapsing four-fold symmetric bubble and a bubble placed within a pure straining flow. The features examined were maximum curvature and deformation of the bubble, and patterns in the evolution of surfactant concentration. The simulations consistently demonstrated that the presence of surfactant facilitates the formation of cusps by reducing surface tension.

Analytical solutions of the type produced by Tanveer and Vasconcelos [26] are delicate and restricted to certain symmetries. The symmetry of the collapsing four-fold bubble was forced, though the surfactant distribution may not have shared its symmetry. This problem comes as a consequence of assuming a truncated polynomial form for bubble shapes. This form is not capable of capturing the effects of irregular patterns of surface tension. Careful attention must be paid to the symmetry restrictions of an analytical solution in order to obtain an accurate result when surfactant is involved.

When computing surfactant, there is a danger of computing non-physical solutions. In the third simulation of a collapsing bubble, the surface tension became negative, causing the surfactant concentration to fall mysteriously. This problem is identified with an inadequate equation of state; smaller β values should be chosen, or perhaps a non-linear equation of state.

One of the drawbacks with using a pseudo-spectral method became patently obvious while attempting to approach a steady-state by computing time-dependent solutions of a bubble placed in pure straining flow. The number of marker points needed to accurately resolve surfactant concentration at later times make such a calculation impractical. Better

suited computational methods may enable further time-dependent investigations of surfactant caps and cusp formation.

The methods employed here are nevertheless effective in computing bubbles to moderate times with simple initial surfactant distributions (Λ_0). Highly accurate solutions are readily obtained when $\Lambda_0 = 1$ (so that symmetry is preserved) and β is small (so that the equation of state leads to physical solutions).

The next step in this work is to incorporate surfactant into a general purpose solver, such as that described in [15]. The analytical solutions developed here would be useful as cases for comparison. In addition, experimentation with more advanced far-field flows involving non-linear terms might prove helpful in developing other solutions with cusp-like features. Investigating alternative equations of state may develop the physical accuracy of the model. Finally, the symmetry constraints on surfactant concentration (Λ) should be investigated if computing with non-uniform initial distributions.

Bibliography

[1] M. Abramowitz, and I. A. Stegun (Eds.), "Complete Elliptic Integrals of the First and Second Kinds" (17.3) *Handbook of Mathematical Functions with Formulas, Graphs, and Mathematical Tables*, 9th printing (Dover, New York, 1972).

[2] D. J. Acheson, *Elementary Fluid Dynamics* (Oxford U., Oxford, 2000).

[3] L. K. Antanovskii, A plane inviscid incompressible bubble placed within a creeping viscous flow: formation of a cusped bubble, *Eur. J. Mech. B/Fluids* **13**, 491 (1994).

[4] J. D. Buckmaster and J. E. Flaherty, The bursting of two-dimensional drops in slow viscous flow, *J. Fluid Mech.* **60**, 625 (1973).

[5] R. L. Burden and J. D. Faires, *Numerical Analysis*, sixth edition, (Brooks/Cole, Pacific Grove, 1997).

[6] George F. Carrier, Max Krook, and Carl E. Pearson, *Functions of a Complex Variable* (McGraw-Hill, New York, 1966).

[7] Tony F. Chan and Luminita A. Vese, Active Contours Without Edges, *UCLA Internal Report*, December 1998.

[8] J. Carrier, L. Greengard, and V. Rokhlin, A fast adaptive multipole algorithm for particle simulations, *SIAM J. Sci. Statist. Comput.* **9**, 669 (1988).

[9] R. A. De Bruijn, Tipstreaming of drops in simple shear flows, *Chem. Eng. Sci.* **48**, 277 (1993).

[10] A. Frumkin and V. Levich, *Zh. Fiz. Khim.* **21**, 1183 (1947).

[11] H. P. Grace, Dispersion phenomena in high viscosity immiscible fluid systems and application of static mixers as dispersion devices in such systems, Chem. Engrg. Commum., *J. Fluid Mech.* **14**, 225 (1982).

[12] L. Greengard, M. C. Kropinski, and A. Mayo, Integral Equation Methods for Stokes Flow and Isotropic Elasticity in the Plane, *J. Comp. Phys.* **125**, 403 (1996).

[13] Thomas Y. Hou, John S. Lowengrub, and Michael J. Shelly, Removing the Stiffness from Interfacial Flows with Surface Tension, *J. Comp. Phys.* **114**, 312 (1994).

[14] Robert A. Johnson and Ali Borhan, Stability of the shape of a surfactant-laden drop translating at low Reynolds number, *Phys. Fluids* **12**, No. 4, 773 (2000).

[15] M. C. A. Kropinski, An Efficient Numerical Method for Studying Interfacial Motion in Two-Dimensional Creeping Flows, *J. Comp. Phys.* **171**, 479 (2001).

[16] M. C. A. Kropinski, Numerical Method for Multiple Inviscid Interfaces in Creeping Flows, *J. Comp. Phys.* **180**, 1 (2002).

[17] H. Lamb, *Hydrodynamics*, (Cambridge U. Press, Cambridge, 1993).

[18] W. E. Langlois, *Slow Viscous Flow* (Macmillan Co., New York, 1964).

[19] S. G. Mikhlin, *Integral Equations* (Pergamon, London, 1957).

[20] S. G. Muskhelishveli, *Some Basic Problems of the Mathematical Theory of Elasticity* (Noordhoff, Groningen, 1953).

[21] C. Pozrikidis, Numerical Studies of cusp formation at fluid interfaces in a Stokes flow, *J. Fluid Mech.* **357**, 29 (1998).

[22] F. D. Rumsheidt and S. G. Mason, Particle motions in sheared suspensions XII: Deformation and burst of liquid drops in shear and hyperbolic flow, *J. Coll. Int. Sci.* **16**, 238 (1961).

[23] Michael Siegel, Influence of Surfactant on Rounded and Pointed Bubbles in Two-Dimensional Stokes Flow, *Siam J. Appl. Math.* **59**, No. 6, 1998 (1999).

[24] Michael Siegel, Cusp formation for time-evolving bubbles in two-dimensional Stokes flow, *J. Fluid Mech.* **412**, 227 (2000).

[25] H. A. Stone, A simple derivation of the time-dependent convective-diffusion equation for surfactant transport along a deforming interface, *Phys. Fluids A* **2**, 111 (1990).

[26] Saleh Tanveer and Giovani L. Vasconcelos, Time-evolving bubbles in two-dimensional Stokes flow, *J. Fluid Mech.* **301**, 325 (1995).

[27] G. I. Taylor, The formation of emulsions in definable fields of flow, *Proc. R. Soc. Lond. A* **146**, 501, (1934).

[28] Harris Wong, David Rumschitzki, and Charles Maldarelli, On the surfactant mass balance at a deforming fluid interface, *Phys. Fluids A* **8**, 3203 (1996).